Physics – Uspekhi **67** (9) 866 – 887 (2024)

REVIEWS OF TOPICAL PROBLEMS

PACS numbers: 87.10.xj, **87.55. – x, 87.56. – v**

ON THE 90TH ANNIVERSARY OF THE P.N. LEBEDEV PHYSICAL INSTITUTE (LPI)

Current status and development of nuclear physics methods of proton therapy at the Lebedev Physical Institute

I N Zavestovskaya, A V Kolobov, V A Ryabov

DOI: https://doi.org/10.3367/UFNe.2024.04.039676

Contents

Abstract. The review is devoted to the development of promising new technologies for diagnostics and radiotherapy in oncology using the Prometheus proton therapy complex based on the Lebedev Physical Institute proton synchrotron. The technologies of proton radiography and tomography, proton therapy with a scanning 'pencil' beam taking into account the intrafractional movement of a tumor, are presented. The results of research in the field of developing new binary technologies for sensitization of proton therapy using targeted nanoparticles are undergoing evaluation at the Russian proton therapy complex at the A Tsyb Medical Radiological Research Center — a branch of the National Medical Research Radiological Centre of the Ministry of Health of the Russian Federation, which ensures the implementation of developed technologies in medical practice. Optimization of the modes is achieved with the support of mathematical modeling of nuclear reactions and sensitization reactions in proton therapy. A project for upgrading the Prometheus proton therapy complex for irradiating tumors of various localizations is presented.

Keywords: proton therapy, nuclear physics methods, intrafractional tumor movement, proton radiography, radiosensitizers, nanoparticles, tumor therapy

I N Zavestovskaya [a], **A V Kolobov** [b], **V A Ryabov** [c]
Lebedev Physical Institute, Russian Academy of Sciences,
Leninskii prosp. 53, 119991 Moscow, Russian Federation
E-mail: [a] zavest@sci.lebedev.ru, [b] kolobov@lpi.ru,
[c] ryabov@lebedev.ru

Received 4 March 2024, revised 28 March 2024
Uspekhi Fizicheskikh Nauk **194** (9) 917 – 940 (2024)
Translated by V L Derbov

1. Introduction

Modern radiotherapy, i.e., treatment with ionizing radiation, in recent decades has undergone revolutionary changes and become an efficient method of high-technology medicine in the treatment of socially significant diseases, including many kinds of oncologic diseases [1–5]. According to data from the World Health Organization, by 2030, cancer morbidity is expected to grow by 70% throughout the world [6, 7]. In 2022, in the Russian Federation, 624,835 cases of primary malignant neoplasms were revealed, which is 7.6% more than in 2021 [8]. Radiotherapy is a proper alternative to surgical interference, e.g., in the treatment of many tumors in the head and neck, cervix, bladder, prostate, and skin. According to world statistics, radiotherapy is recommended to more than 70% of patients solely and/or in combination with other methods of oncological treatment.

Many kinds of radiotherapy with improved accuracy have appeared, such as gamma-knife, cyber-knife, as well as various options of conform radiotherapy. However, there is one disadvantage in the application of conventional radiotherapy methods. The radiation consists of a beam of photons and electrons, which damage not only the tumor but also healthy tissues located in front of and behind the tumor along the radiation beam. As a result, damage to healthy tissues occurs, and side effects arise. To reduce their influence and to avoid fatal damage of healthy tissues, it is necessary to restrict the radiation power applied to the tumor [4]. In addition, the use of gamma radiation along with X-ray radiation in the treatment of patients with malignant tumors has substantial limitations: the maximum dose falls on the skin and adjacent healthy tissues, whereas the tumor itself in most cases is localized deeper. To reduce the effect of radiation on healthy

tissues, the irradiation of a tumor from different directions and using fields of complex spatial configurations (IMRT/IGRT/VMAT) are used [2, 3]. Unfortunately, even these do not always allow applying the required therapeutic dose to the tumor without damaging the surrounding healthy tissues and organs of critical importance [4].

Proton therapy (PT), in which a beam of protons is used to irradiate the affected organ, is an up-to-date, high-tech, and virtually risc-free method of radiotherapy [1, 3]. Throughout the world, PT is distinguished as one of the most promising methods of radiation treatment of oncological diseases [2, 4]. A specific feature of proton radiation is that the main energy of the beam of protons is released at a certain depth of the organism tissue. The depth of the irradiated tissue layer is determined by the energy of the proton beam, and the part of the dosage distribution having a maximum at a certain point is called the Bragg peak [9]. The main advantage of proton radiation consists in the possibility of precise localization of the irradiated site, the radiation load on the healthy tissues being decreased compared to usual X-ray or gamma radiotherapy (Fig. 1). A medical radiologist devises the plan of irradiation in such a way that the energy is released exactly in the tumor, repeating its contour with an accuracy of a millimeter. Thus, only the tumor located rather deep is destroyed, and the surrounding healthy tissues are virtually unaffected by the radiation. PT allows irradiation of tumors located near organs, the irradiation of which is related to a high risk of damage. Pediatric oncology, as a rule, does not allow using conventional radiotherapy, and only PT can be used in most cases [10].

The depth distribution of a dose for various kinds of ionizing radiation (see Fig. 1) shows that the dose maximum in the case of photons and electrons (I, II, III, IV) goes to a relatively small depth, whereas protons (or heavier ions, e.g., ^{12}C) offer more chances of forming a localized dose distribution. Moreover, the dose after the Bragg peak is insignificant, while the photons completely pass through the patient's body, and the total energy released in the patient's body (often referred to as the integral dose) in PT is usually a third or less than in any other kind of photon therapy.

Hadron therapy — therapy using charged particles (protons or ions) — promises to become a leading approach in the world in noninvasive treatment of various forms of cancer in the first decades of the 21st century [11–13]. This is confirmed by the almost exponential growth of the number of hadron therapy centers operating and under construction in the world during the last decades, which is related to the change in the concept of patient treatment: from using facilities of research centers to creating specialized medical centers. By the beginning of 2024, according to data from the Particle Therapy Co-Operative Group (PTCOG), in the world there are 129 medical centers for hadron therapy, including 46 in the USA, 26 in Japan, 28 in Europe, 8 in China, and 4 in Russia [14]. Taking into account Russian Federation statistics, 33 more centers are under construction and 35 are being planned in the world. Thus, in 2030, throughout the world, there will be 196 centers of hadron therapy, including 175 centers of PT. This is because the cost of facilities for therapy with carbon ions is quite high, which hampers their mass use in the therapy of oncological diseases [2].

In Russia, till relatively recently, the treatment of patients by a proton beam was implemented in physics research institutes, using facilities intended for physics experiments.

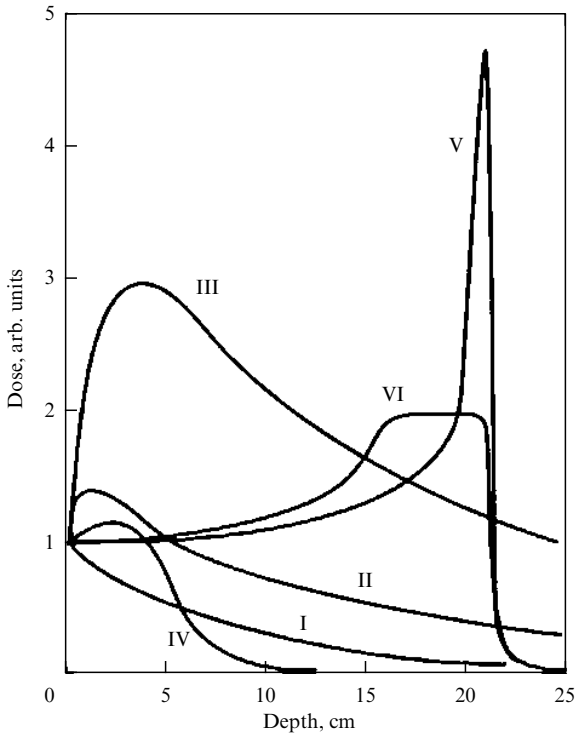

Figure 1. Dependence of dosage on penetration depth into the tissue for X-ray radiation (200 kV) (I), radiation of ^{60}Co (II), high-energy photons (nominal 22 MeV) (III), electrons (22 MeV) (IV), protons (200 MeV) (V), modified Bragg peak (VI).

Since 1969, more than 4,300 patients have been treated with the therapeutic beam at the A I Alikhanov Institute of Theoretical and Experimental Physics (ITEP, now the National Research Center Kurchatov Institute, Kurchatov Complex of Theoretical and Experimental Physics) [15]. Due to a fire in 2012, the ITEP accelerator was shut down [16]. The Medical Technologies Complex based at the Laboratory of Nuclear Technologies of the Joint Institute for Nuclear Research continues to operate; since 1967, more than 1300 patients have been treated there [17, 18]. Currently, it does not operate as a medical facility, but can serve up to 50 patients per year [3, 5]. At the B P Konstantinov Petersburg Nuclear Physics Institute (PNPI) in Gatchina, a medical facility was created based on a 1-GeV synchrotron that specializes in the treatment of small head tumors and eye melanoma using the through-beam method. Over the 40 years of its existence from 1975 to 2015, more than 1300 patients were treated with this beam [19].

In the Russian Federation from 2015 to 2019, four specialized proton medical centers were put into operation. Two of them use the Prometheus proton therapy complex (PTC) (Fig. 2), which was created at the Physics and Technology Center of LPI (PTC LPI, Protvino, Moscow Region) in the early 2000s under the supervision of V E Balakin.

The Prometheus PTC was created based on the latest achievements of science and technology and, in terms of its technical and operational characteristics, is currently one of the best in the world [20]. The first production model of the complex was launched in Protvino in a special building of the city hospital in 2015. In 2017 a registration certificate for a medical device was received [20]. The first hospital model of the Prometheus PTC was installed in Obninsk (Kaluga

Figure 2. Photograph of proton synchrotron of Prometheus PTC.

Region) in the country's leading radiology center, the A F Tsyb Medical Research Center, a branch of the National Medical Research Center of Radiology of the Ministry of Health of the Russian Federation, which has been treating cancer patients since 2016 [21]. To date, more than 800 patients have been successfully treated using it [22–26]. An assessment of the throughput capacity of one Prometheus complex conducted at the National Medical Research Center of Radiology shows the possibility of treating up to 450 patients per year.

Proton beam treatment in the Russian Federation is carried out at two more centers using foreign-made facilities. The American Varian-ProBeam proton complex was launched in October 2017 at the Sergei Berezin International Institute of Biological Systems (IIBS) in St. Petersburg [27]. This is the first private proton medical center in Russia, which allows treating 800 patients per year. A proton complex based on the C235-V3 cyclotron (IBA, Belgium) with a maximum beam energy of 235 MeV (created with the participation of JINR, Dubna) was launched in September 2019 in Dimitrovgrad (Ulyanovsk region) [28]. This center provides treatment for oncological diseases of all localizations with a throughput of 1200 patients per year.

As a part of implementing the Federal Scientific and Technical Program for Synchrotron and Neutron Research and Research Infrastructure for 2019–2027, three new specialized medical centers for hadron therapy are at the design and construction stage in Russia. A plan to create a proton therapy center is being implemented at the Moscow site of the Kurchatov Institute National Research Center. A synchrotron is being developed to accelerate a proton beam to an energy of 70–250 MeV. The beam intensity will be 5×10^{10} protons per second, and the maximum size of the dose field will be 25×25 cm. The developed pulsed proton accelerator with spatially homogeneous quadrupole focusing (RFQ) for an energy of 5 MeV with an operating frequency of 162.5 MHz and a current of 30 mA will be used as an injector. The proton therapy complex implies the creation of two compartments for irradiating patients, with a gantry system and a horizontal fixed beam. The start of medical care at the facility is planned for 2030. A plan to create a PT complex for oncoophthalmology is being implemented in Gatchina (Leningrad Region) based on the modernization of the C-80 cyclotron of the Kurchatov Institute National Research Center–B P Konstantinov Petersburg Nuclear Physics Institute. The proton beam energy at the cyclotron output will be 70 MeV, and the cross-sectional diameter will be 60 mm. The beam divergence will be no more than 60 mrad, and the unevenness of the particle density across the beam cross-section will be no more than $\pm 3\%$. This complex will be able to provide treatment for patients with tumors of the visual organs, as well as to test domestic technologies for PT of malignant neoplasms of the eyes and adnexa. The commissioning of the complex and obtaining of a medical license are planned for 2024, with the start of medical care in 2025. The creation of the ion (carbon) radiation therapy complex is being implemented based on the National Research Center Kurchatov Institute, Institute for High Energy Physics (Protvino). The energy of the carbon ion beam will be 200–450 MeV per nucleon, while the intensity will be up to 10^9 s^{-1}. A system for slow beam extraction with a duration of 1–2 s is being developed, and the beam nonuniformity will be no more than 2.5%. The start of medical care is planned for 2029.

According to the oncology community, at least 50,000 patients per year in Russia need PT [29]. However, the existing PT centers and those under construction in the Russian Federation can provide treatment for no more than 3500 patients per year. It is necessary to improve domestic proton therapy complexes, ensure their production at Russian enterprises and placement in medical centers to make proton therapy available in the Russian Federation, as well as develop and implement new methods of proton and ion therapy in medical practice to ensure the effectiveness of the treatment of socially significant diseases. Today, when the supply of medical equipment from abroad is under threat and there is a problem with its maintenance and repair in the Russian Federation, the production of domestic high-tech medical equipment is becoming a critical issue for the country. Therefore, the development and implementation of new PT technologies, which give impetus to further replication of hadron therapy complexes, including the Prometheus PTC, are an important step towards import substitution in the field of high-tech medical care.

2. Prometheus proton therapy complex

2.1 LPI proton synchrotron and Prometheus proton therapy complex

The Prometheus complex is a unique domestic development. It is based on a compact (outer diameter 5 m, weight 15 t) proton synchrotron with low energy consumption (up to 100 kW) (see Fig. 2) [30]. The manufacturer of the Prometheus complex is the Russian company JSC Protom, which was founded in 2001 for the mass production of proton accelerators based on the scientific developments of the Lebedev Physical Institute. The high working cycle of the installation is achieved due to rapid acceleration to maximum energy with an extraction cycle of up to several seconds. The intensity of the proton beam is, on average, 10^9 particles per cycle of complete beam extraction. The energy of the therapeutic beam can vary from 30 to 280 MeV. The beam diameter at the tumor location is several millimeters.

The Prometheus proton synchrotron is significantly cheaper both in production and maintenance than its Western counterparts (Varian and IBA); it is cost-effective and requires minimal operating costs and personnel. All this, with productivity comparable to competitors, provides great advantages on the world market. Currently, proton synchrotrons produced in Russia by JSC Protom have been commissioned and are being put into operation for the treatment of patients in foreign centers in Europe, Israel,

China, the USA, and Australia. In the USA, two proton synchrotrons with an American medical unit were delivered to the McLaren Clinic (Flint, Michigan) and the Massachusetts General Hospital (Boston, Massachusetts). In total, several hundred people have already undergone treatment with them in the United States. A facility has been launched in Israel that provides treatment in a sitting position.

The Prometheus PTC was created by Russian scientists for the most precise, dosed proton targeting of malignant neoplasms localized inside healthy tissue with minimal injury to the latter. Using the complex for PT tasks allows increasing the level of local control in the treatment of patients with malignant neoplasms, reducing the frequency and severity of post-radiation complications, and irradiating tumors located close to critical organs and structures.

The advantages of the Prometheus PTC are not only its compactness but also the ability to perform three-dimensional conformal irradiation of the tumor using active modulation of the Bragg peak, the presence of an original system of vertical positioning and fixation of the patient, allowing irradiation at an angle of 0°–360°, as well as a unified automated system for irradiation. The irradiation time of tumors of the most common volumes is about 10 minutes. To control the patient's position before the radiation therapy session, a series of X-ray projections are taken from different directions with subsequent adjustment of the patient's sitting position. Due to this, an accuracy of about 0.3 mm is achieved. A possible deviation from the required position is clearly visualized and then corrected using a built-in computer tomograph.

Today, the main irradiation mode on the Prometheus PTC is irradiation in a sitting position. The advantages of this mode are the ease of patient fixation and the possibility of using a fixed beam. During a session of irradiation with a horizontal scanning proton beam, the patient is positioned in a special chair (Fig. 3) that can move around its axis, which allows a unique approach to tumor irradiation in 1–36 directions per session, depending on the irradiation plan. Before the irradiation session, the medical staff immobilizes (fixes) the patient and leaves the room where the irradiation is executed. During irradiation, the radiologist and the patient are in contact via video and audio communication. After completion of irradiation, the medical staff releases the patient from the fixing devices and directs them to auxiliary rooms.

Various authors have shown that the use of a fixed proton beam output, together with an immobilization system in a sitting position, is a promising technology [31–36]. In this position, the displacement of internal organs occurs to a lesser extent, which allows a smaller irradiation area, thereby reducing the load on healthy tissues [34]. Clinicians at the A F Tsyb Medical Radiological Research Center (MRRC), a branch of the National Medical Research Center of Radiology of the Ministry of Health of the Russian Federation, have accumulated eight years of experience using this technique for irradiating neoplasms located in the head and neck: brain tumors, tumors in the skull base, pituitary tumors, and eye melanoma [22–26]. Focus on the use of modern automated and robotic means of immobilization and patient positioning made it possible to abandon the use of bulky and expensive magnetic proton beam positioning systems such as a gantry. In addition, in March 2017, the medical Prometheus PTC (Obninsk) was licensed for irradiation of the entire human body in a lying position. Currently, medical studies are underway on the possibility of using a specialized table designed by JSC Protom to ensure the patient's lying position, which will allow irradiation of tumors of all possible organs and localizations.

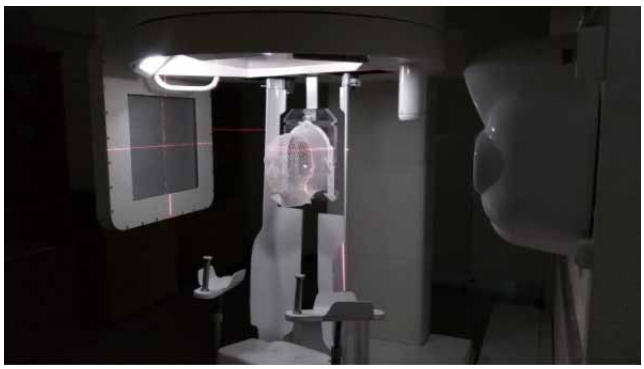

Figure 3. Treatment room of the complex: armchair for patient irradiation in the sitting position.

Figure 4. Photograph of assembly shop of JSC Protom (Protvino).

According to the creator of the Prometheus PTC V E Balakin, "we can affect a tumor of any complexity, mass and genesis and destroy it. In oncology, it is often like this: you seem to have suppressed the tumor, but it grows again. Our beam is so thin that it allows us to irradiate the tumor radically, even if it borders on sensitive areas. You only need to 'tell' this to the computer that plans the irradiation and supply the area with a dose to destroy the tumor." JSC Protom has the capacity to produce at least three Prometheus complexes per year. Figure 4 shows the shop where proton synchrotrons are assembled.

2.2 Technologies of proton therapy with a scanning beam. Considering tumor intrafractional movement

A proton beam at the accelerator output is usually a narrow (up to 7–8 mm) monoenergetic beam with a Gaussian shape. Without subsequent modification, such a beam is unsuitable for clinical use due to uneven energy distribution. Formation of a therapeutic proton beam is carried out by two methods: the passive scattering method and the pencil beam method.

The passive scattering method is commonly used to treat ophthalmological diseases [37]. A narrow proton beam from an accelerator is modulated (expanded) using a scattering system, the main task of which is to create a region of a relatively uniform plateau in the cross section. Typically, thin (tens of micrometers) tantalum foils are used for these purposes. The beam then passes through a comb filter, which allows creating an absorbed dose plateau of a given length, i.e., the spread-out Bragg peak (SOBP). If it is necessary to reduce the energy and ranges of protons, the beam is directed to an absorber (degrader). When using a rapidly rotating absorber with individual increments for its thickness to reduce energy, the spread-out Bragg peak can be obtained in one revolution. The width of the absorber increment is responsible for the energy density of the beam and, therefore, the height of each Bragg peak. Such rotating absorbers ('range modulator wheels') act as a propeller with blades through which the beam passes, with the thinnest blade providing the largest interval of the action range. Conformity of irradiation, i.e., the correspondence of the dose distribution to the shape of the pathological volume of the target irradiation area, in the plane perpendicular to the beam axis is ensured by a collimator. Adjustment of the distal dose distribution considering the heterogeneity of the patient's body, unevenness of the surface, and the need to preserve healthy tissue is executed by a compensator. It is worth noting that, in the case of photon therapy, this is possible only by setting several irradiation directions [4].

However, the passive scattering method has its limitations from the point of view of dose formation. For example, the distribution cannot be conformal to the proximal surface of the target. Moreover, the scattering and collimation system usually provides a beam efficiency of about 3–15%. Therefore, there is a tendency to switch proton planning and delivery strategies to scanning pencil beam PT technology.

Scanning beam PT technology enables the formation of a dose distribution by magnetic scanning of narrow pencil beams with a Gaussian shape and thus individual Bragg curves, the 'beamlets.' Individual proton beams with a width (sigma) of a few mm (usually about 2–10 mm, depending on the beam energy and delivery system) scan the tumor layer by layer using a changing magnetic field in the x and y directions (Fig. 5). Since the tumor can be scanned with narrow pencil beams, there is no need for a scattering system for lateral field expansion, as is the case with the passive scattering method. This results in a sharper Bragg peak when using the scanning beam than with the passively scattered beam. The efficiency of the scanning delivery system is close to 100%.

The scanning depth is controlled by changing the beam energy, as in the passive scattering technique. However, the individual beam energy for each pencil beam set is controlled separately rather than by a modulator. The proton beam energy is usually adjusted outside the treatment room. The time required to change the energy depends on the accelerator and delivery system and is an important clinical parameter, since it determines the duration of the treatment as well as the uniformity of the dose due to possible involuntary patient movement. For very low proton energies or for precise tuning of the energy, absorbers or apertures can also be integrated into the treatment head to improve the lateral penumbra of the field. Pencil beam scanning involves irradiating the tumor in isoenergetic layers with energy increments depending on the setup and treatment plan, as well as the distance between the layers of scanning.

Narrow pencil beam scanning technology is implemented in the Prometheus PTC. With a beam energy of about 150 MeV (one of the most frequently used energy values for therapy), the size of the proton beam in the orthogonal plane is no more than 3 mm.

One of the main areas of development of scanning beam PT technology is the treatment of moving tumors [40]. Intrafractional movement of a tumor and the surrounding organs and tissues is movement right during the irradiation session. The movement is induced to the greatest extent by the patient's breathing, its amplitude ranges from units to tens of millimeters and depends on the organ, and the characteristic period is several seconds [38]. Intrafractional movement leads to distortion of dose distributions, the appearance of over- and under-irradiation areas, and a violation of conformity, which significantly reduces the effectiveness of PT [39]. This problem has already been solved in photon radiation therapy [40], but direct transfer of methods for reducing and compensating for the effect of intrafractional movement to PT is difficult and requires a revision of existing approaches and methods, additional research, and the development of new approaches [38–40]. The difficulties are caused, first, by a significant difference in the process of interaction of the scanning therapeutic proton beam with the patient's organs and tissues. Distortions of the dose distribution formed during target volume irradiation in the active scanning mode are caused not only by translational displacement, as in the case of photon therapy, but also by changes in the density

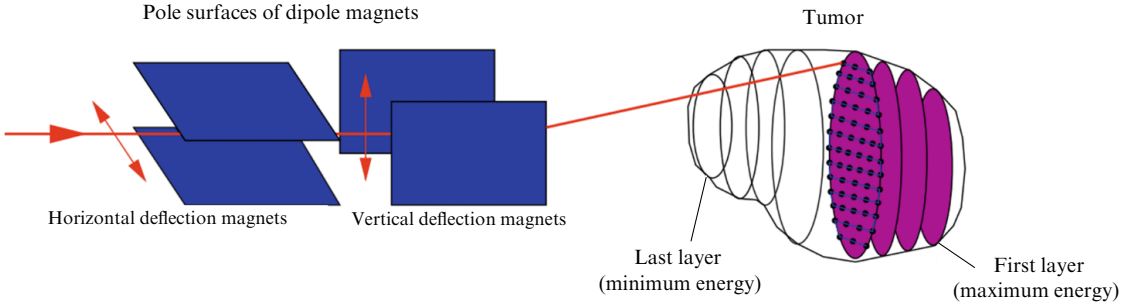

Figure 5. Schematic diagram of proton beam formation with pencil beam scanning technology.

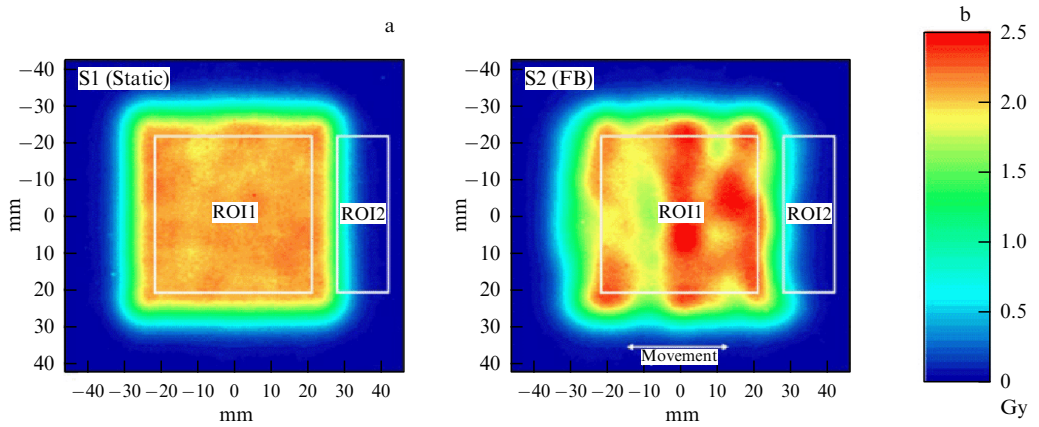

Figure 6. Graphic images of transverse dose distributions in fixed (S1, Fig. a) and moving (S2, Fig. b) targets in free breathing (FB) mode. RO11 is region of interest 42 mm × 42 mm in size, equivalent to contour of clinical target volume (CTV); RO12 is region of interest 42 mm × 14 mm in size, corresponding to nearest risk organ [53].

along the beam path and desynchronization between the movement of the target volume and the movement of the beam. In addition, tumor movement is usually a superposition of translational, rotational movement and deformation, which also affects the process of irradiation with a scanning beam of protons. Solving the problem of accounting for intrafractional tumor movement in PT with a scanning beam will expand the scope of its application to localization of the chest and abdominal cavity: lung cancer [41, 42], breast cancer [43], prostate cancer [44], liver cancer [45], etc.

The greatest contribution to the study of the intrafractional motion effect in hadron therapy, the development and implementation of motion compensation methods in clinical practice, was made by the research teams of the GSI Helmholtz Centre for Heavy Ion Research (Darmstadt, Germany) and the Proton Beam Therapy Center, Hokkaido University (Japan). At GSI, the effect of motion on dose distribution was experimentally studied [39, 40], an approach to 4D treatment planning was developed [46], and gating and tracking technologies were created for carbon ion therapy [47–49]. At Hokkaido University, research is being conducted in the field of proton therapy of mobile tumors in the gating mode with motion control using radiopaque markers and an X-ray system (Real-time-image Gated Proton Therapy) [50, 51]. It should be noted that existing technologies and treatment methods that take tumor motion into account are experimental in nature [39, 40].

Solving the problem of intrafractional movement in PT requires close cooperation of various specialists: radiologists, medical physicists, and engineers. The LPI team has many years of experience working with a proton synchrotron specialized for PT, in conducting dosimetry and radiobiological studies, as well as in developing proton therapy planning systems for clinical practice.

A series of studies on the Prometheus PTC to improve the technologies of PT with a scanning pencil beam, as well as dosimetric studies of the optimal scanning method and the effect of radiopaque markers on the dose distribution, were carried out. Experiments on modeling the intrafractional movement of the target in various modes were implemented using the water dynamic phantom developed for solving PT problems and optimized for the parameters of the Prometheus PTC. A high-speed optical respiration sensor was developed that allows real-time noncontact recording of the patient's breathing without installing additional markers on the patient's chest. Equipment is currently being developed to implement another promising method of monitoring the patient's breathing based on bioimpedance analysis, tested and recommended for use in radiation therapy [52].

In Ref. [53], the effect of intrafractional movement on dose distributions in the target during PT with a scanning beam on the Prometheus PTC was studied. The study was conducted by qualitatively analyzing the structure and shape of dose distributions, as well as quantitatively analyzing the average dose and dose homogeneity within the region of interest (target irradiation region) for different motion parameters and accelerator operation cycles. It was found that intrafractional motion leads to significant distortion of the shape and structure of the dose field. The distortions are expressed in the appearance of 'hot' and 'cold' spots, i.e., areas of over- and under-irradiation, respectively, and the blurring of the dose field along the motion trajectory (Fig. 6). These effects are reflected in a decrease in the average dose in the region of interest by 16% and dose homogeneity from 96.7% to 75.5% as the motion amplitude increases from 0 to 10 mm. The level of distortions in this case weakly depends on the time parameters of motion and the accelerator operation cycle.

Thus, it was shown that the observed effects of dose field distortion led to a decrease in the efficiency of TP in the treatment of moving tumors. The development and application of such motion compensation methods as multiple scanning (rescanning), deep breath-hold therapy, the gating method, as well as combinations of these methods, are important tasks for clinical practice.

Rescanning is a specific method that is used only in scanning beam therapy. It consists of multiple repeated irradiations of the tumor volume, which leads to statistical averaging of the dose. The beam intensity during such irradiation in one scan is equal to the total intensity divided by the specified number of repetitions N. The prescribed dose will be delivered to the target volume when the specified number of repeated scans N is completed.

Deep inhalation breath hold (DIBH) is one of the most common and effective methods of active motion compensation. This method involves providing a sufficient beam at times when the patient holds their breath, so that the tumor is in approximately the same position and remains virtually motionless. This method is actively used for left-sided breast cancer, as it allows minimizing the dose to the heart by

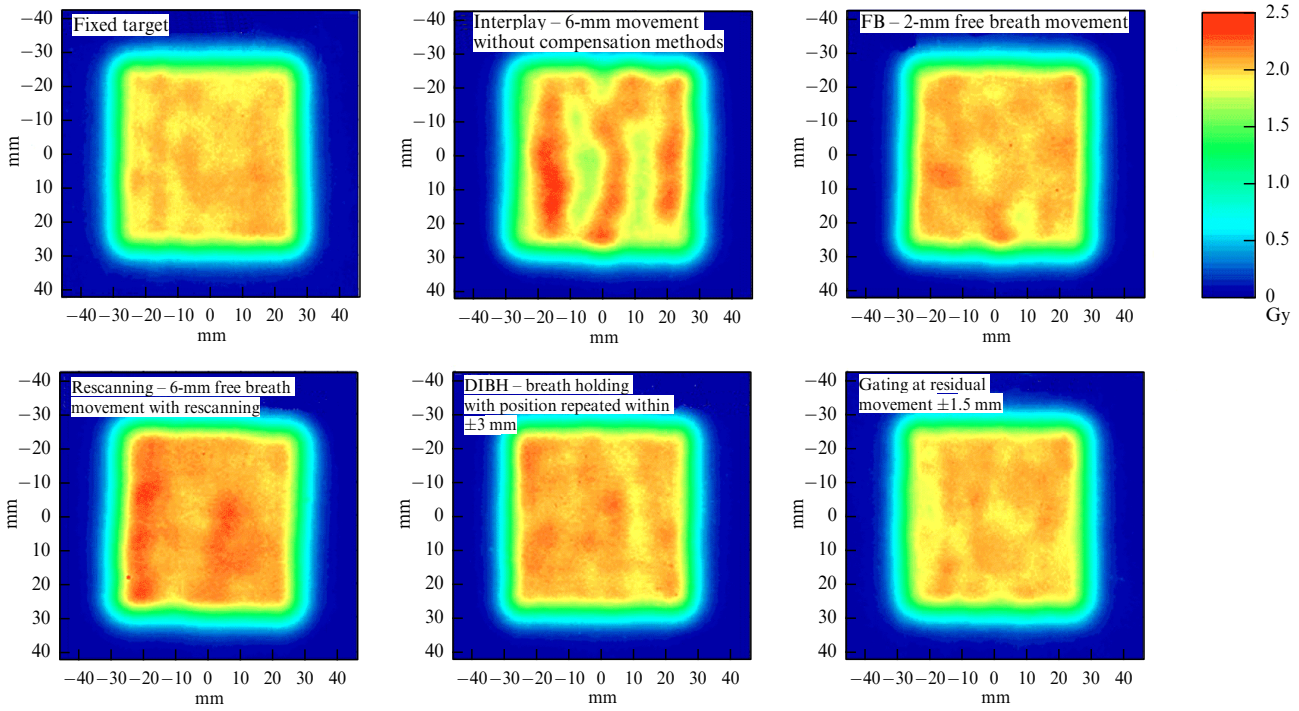

Figure 7. Dose distributions in fixed and moving targets in various irradiation modes.

maximizing the distance between the heart and the mammary gland in both photon and proton therapy.

Unlike the breath-holding method, gating implies irradiating a moving target while breathing freely, with the beam being delivered only at a specific, predetermined phase of the movement. The phase is chosen so that in each cycle of movement the tumor in this phase is in the same most stable position. The gating window is chosen, on the one hand, as wide as possible to minimize the treatment time. On the other hand, the width should be such so as to minimize residual movement within the gating window.

A technology for planning PT in the multiple scanning mode was developed on the Prometheus PTC. The technology was implemented at the A F Tsyb MRRC and is widely used to conduct *in silico* studies using water-equivalent and anthropomorphic phantoms, as well as models of biological objects. The behavior features of the expected beam extraction characteristics and the limits of acceptable uncertainties of the final distribution of absorbed doses are studied. After bringing the characteristics of the synchrotron control hardware and software in line with the requirements described in the technological instructions, the technology can be fully implemented in the routine clinical practice of PT of patients with moving targets within the limitations presented in the technological instructions. The expected effects of the implementation are a significant increase in the homogeneity of covering moving targets and a reduction in the uncertainties of absorbed doses both in the target and in the areas of interest (for example, critical organs). Among the minor disadvantages, one can highlight the increase in session duration; however, innovative methods implemented within the technology allow achieving an increase in session time of no more than 20% of a traditional session, while classical schemes used around the world for such solutions imply an increase in session time of up to 150%.

In addition, a module of the planning program was developed for the medical physicist to create a file of the training plan for moving targets using the multiple scanning method with specified parameters. This module was integrated into the Protom Planner planning program; it allows forming a uniform field in the target when irradiating moving objects using the Prometheus PTC. Two methods of multiple scanning were developed for use on various irradiation targets: fixed, which continually repeats uniform irradiation of the entire target volume, and adaptive, repeating irradiation of those zones that have the greatest effect on the uniformity of the dose distribution.

The efficiency of using the rescanning, DIBH, and gating methods on the Prometheus PTC was compared (Fig. 7). It was shown that, with a motion amplitude of less than 2 mm, irradiation can be performed in free-breathing mode using no methods of motion compensation. With a motion amplitude of 2 to 6 mm, the use of multiple scanning technology is recommended, but optimization is required to minimize the irradiation time. With a motion amplitude of more than 6 mm, the use of the DIBH or gating method is recommended, but it is necessary to measure the repeatability of the tumor position (for DIBH) or select the optimal window width (for gating). It is shown that gating is the most effective method for the Prometheus PTC from the point of view of optimizing the distribution of the absorbed dose and irradiation time.

The new operating mode of the Prometheus proton synchrotron in the gating mode is shown in the time diagram, Fig. 8. Its main advantage is that, in addition to the permission to extract the beam, its injection into the ring is also controlled (purple curve). For a sufficiently regular cycle of tumor movement, it is possible to predict the moment at which the injection should be performed, so that, by the expected moment of permission to extract, the beam is already accelerated and ready for extraction. The new

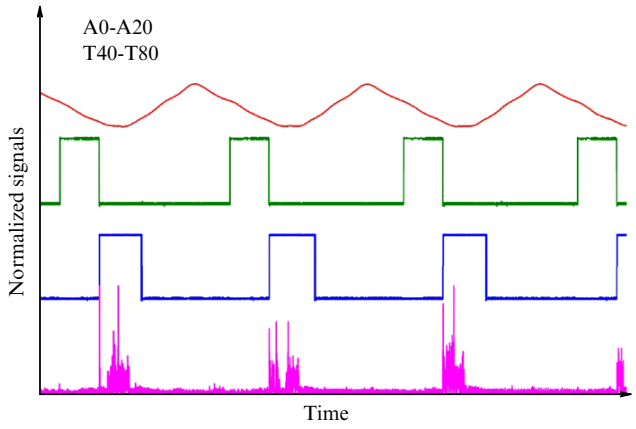

Figure 8. Timing diagram of beam delivery in gating mode using the developed synchronization algorithm. Diagram shows four signals: target motion signal (red curve), beam injection signal (green curve), beam output permission signal (blue curve), and irradiation signal (magenta curve).

approach allows the beam to be extracted immediately after its acceleration, and, with each permission pulse, the beam will be guaranteed to be extracted for the duration of the entire pulse of permission to extract. In addition, the magnetic system is in standby mode most of the time, maintaining the injection field, which eliminates overheating of the system. Further work will be aimed at developing a new system for verifying the position of an object based on a high-power X-ray source and a detection screen mounted on a robotic manipulator, as well as integrating the developed technologies for recording the patient's intrafractional respiration into the proton beam control system on the Prometheus PTC.

2.3 Proton radiography and tomography

The history of proton radiography began in the 1960s. Research was primarily aimed at obtaining radiographic images with better density resolution and at the same time a lower received dose during scanning than with X-ray radiography. Only two decades later, proton radiography and tomography began to be considered methods for directly determining the stopping power of the medium for protons, which is the basis for software dosage planning for PT. This was due to the appearance of the first software packages for dosage planning calculation in photon radiation therapy, and then in PT.

The proton synchrotron of the Lebedev Physical Institute is used to develop a method of proton radiography and tomography. The maximum energy achievable with it, 330 MeV, was specially planned by the developers, as it allows obtaining proton radiographic images of any neoplasm localization in the human body without any restrictions, e.g., for neoplasms in the pelvic region. It should be noted that all medical proton accelerators existing in the world today use energies up to 230–250 MeV. Such values are equivalent to the mean free path of a proton beam in water of approximately 30 cm and cannot be used for proton radiography or tomography.

For protons, a direct method for restoring the stopping power of the medium is proton imaging, which includes proton radiography (one image from one direction) and tomography (multiple images with subsequent restoration of a three-dimensional model of the object under study). Such methods involve the use of the same radiation source that is used for therapy. Proton radiography is a two-dimensional extension of the proton probe method, but, unlike this method, in proton radiography, the coordinate of the entry and exit of each proton from the irradiated object is fixed [54]. This method allows one to determine the position of proton stops in tissues with high accuracy. This can be done for each specific patient immediately before the PT session, thereby significantly increasing the accuracy of PT and virtually eliminating the uncertainties of proton path lengths, which are currently included in all modern therapy planning systems. In addition, proton radiography is free from the disadvantages of the X-ray approach in imaging objects containing metal inserts, which many implants may be, and is essentially the only method that allows imaging such objects without artifacts.

In the 1970s and 1980s, the first series of proton imaging experiments was conducted at the Los Alamos Meson Physics Center, aimed at bridging the gap between physics laboratory experiments and clinical practice. The first experimental system consisted of a high-purity germanium (HPGe) detector and a multiwire proportional chamber to measure the residual energy and exit position of each proton, respectively. A later modification of the same system added a detector consisting of a set of plastic scintillators designed to measure the residual energy of the proton beam. In published papers [55, 56], the minimum dose and the maximum possible counting rate were estimated [57]. The final experiment in this series involved scanning human tissue samples to demonstrate the feasibility of using proton imaging for clinical practice [58]. One of the important conclusions from these early experimental studies was that, to obtain better spatial resolution, it is necessary to know the coordinates of the proton beam at the entrance to and exit from the irradiated object.

There are three research groups in the world that are working on solving problems in the field of proton radiography and tomography: two foreign groups and a Russian team from the Lebedev Physical Institute.

One of the foreign groups includes scientists from the University of Lincoln in the UK, as well as employees of the private company ProtonVDA, together with several research institutes in the USA. The ProtonVDA company [59] has developed a highly efficient and inexpensive proton tomography system based on the rapidly developing technology of fast scintillators. One of the main advantages of this device is the lower dose received by the patient than with similar X-ray imaging systems. This feature is explained by the precise reconstruction of the tracks of individual protons passing through the patient's body, as well as the use of a special accelerator operating mode with an ultra-low intensity of the extracted beam during the entire scanning period.

There is also a project called PRaVDA (Proton Radiotherapy Verification and Dosimetry Applications) [60], which is being carried out by a collaboration of universities in the UK, and experiments are being carried out at the proton cyclotron in South Africa. This project makes extensive use of detector technology used in high-energy particle track reconstruction experiments, such as NA62 at CERN (Switzerland). PRaVDA uses radiation-hardened silicon track detectors to quickly and accurately measure the trajectory of protons as they pass through an irradiated object. A set of track detectors, in combination with a calorimeter for measuring the residual

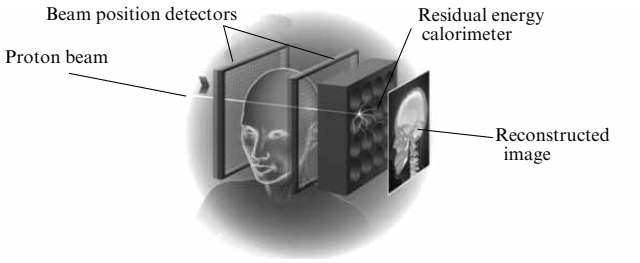

Figure 9. Arrangement of main elements of system for proton imaging of irradiated object.

energy of protons, provides information on the angular deviations and energy losses for each proton. However, to date, none of these detectors is used in clinical practice. One of the key reasons is the need to work with ultra-low proton beam intensities and energies sufficient for the beam to pass completely through the patient's body. The main proton accelerators used for radiotherapy are proton cyclotrons and synchrocyclotrons [61], which are characterized by fixed values of intensity and energy of the extracted beam. These parameters are set at the design stage of the accelerator in accordance with its future application. Thus, for PT, the maximum energy is in the range of 230–250 MeV, and the minimum intensity is from 10^9 protons per second. At the same time, for proton radiography and tomography, energies from 250 to 330 MeV are needed, and the beam intensity is up to 10^6 protons per second.

A system designed to obtain tomographic images using heavy charged particles should consist of detection units capable of determining unambiguously or with a good degree of reliability the position of the proton or ion beam before and after passing through the object of study, as well as a calorimeter determining the residual energy of the beam after irradiation of the object. The system also includes software implementations of image reconstruction techniques, i.e., two-dimensional or three-dimensional maps of the medium stopping power for charged particles. The general operating principle of the proton imaging system is shown in Fig. 9.

Reference [62] describes a proton imaging system containing two planes of beam position detectors located in front of and behind the object under study. The sensitive area of the detectors is 38.4 cm × 38.4 cm. Each plane consists of two layers of thin scintillating cylindrical rods; the layers are shifted by one half, and the spatial resolution of this grating is 1 mm. Each rod is connected by flexible light-conducting cables to an array of solid-state silicon photomultiplier tubes (PMTs) 6 mm × 6 mm in size. A total of 128 PMTs are used. Due to the shift in the layers in the detecting planes, it is possible to determine the beam position with an accuracy of 0.5 mm. Considering the data from the accelerator's scanning magnets, it is possible to calculate the angle at which the protons enter the irradiated object.

In addition to the above-described system based on scintillation sensitive elements as modules for determining the position of the proton beam, there are other approaches to detecting the position before and after the irradiated object. For example, a proton radiography system with an alternative design was developed within the framework of the Italian TERA project [63]. The TERA beam position detector system uses gas electron multipliers (GEMs) with an area of 10 cm × 10 cm to achieve the desired submillimeter spatial resolution. These GEMs use a conductive kapton film coated with copper on both sides. When a voltage of 100–450 V is applied to the copper foils, an electric field is created in the active holes of the films, obtained by acid etching. Although the copper and kapton foils are thin, the high atomic number of copper and the large amount of foil required (the system in question uses three PEMs in a row) will result in significant multiple Coulomb scattering, which reduces the potential accuracy of the system.

The proton residual energy detector described in [62] is a compact scintillator unit measuring 40 cm × 40 cm and 13 cm thick. This scintillator unit has a sensitive thickness of 10 cm, which allows the use of multiple energies when scanning areas of interest. Sixteen 76-mm-diameter vacuum PMTs (Hamamatsu, model R6091) are distributed in a 4 by 4 grid. This grid is attached to the back of the scintillator unit. The sides of the scintillator not covered by the PEMs are painted black to absorb photons.

In another detector design described in [64], the scintillator material chosen was based on polystyrene UPS-923A, which provides high light output, low light absorption, and long-term stability. The thickness of each detector part was 51 mm, and five parts were used in total. The sensitive area was 9 cm × 36 cm. The original idea was to use scintillator plates beveled at an angle of 35° to form a built-in light-guiding plane. All sides of the scintillator were optically polished, and the PMTs were glued to the scintillators with optical epoxy resin. Each scintillator-PMT assembly was coated with a reflective material.

For the Prometheus PTC, a multi-turn mode of ultra-low intensity proton beam extraction from the proton synchrotron, a calibration and verification system, and an embedded extraction control module, as well as a single-proton event detector, were developed to implement efficient detection of single-proton events during radiographic irradiation. The system is integrated with the Prometheus PTC [65–69].

To implement proton tomography, further work is needed to ensure proton beam energy detection, image acquisition, and analysis. All these tasks should be optimized for specific parameters of the Prometheus PTC. Since it is necessary to increase the sensitivity of the beam output control unit when operating with an ultra-low intensity radiographic beam, a scheme for upgrading the accelerator complex was proposed, containing a corresponding new module simultaneously with an updated version of the automated control program for the proton synchrotron, including beam output settings for proton imaging (Fig. 10).

The proposed scheme is based on the current software architecture of the complex control system and will not cause major difficulties during its implementation. Switching between the proton beam output modes from the synchrotron for therapy and imaging will be implemented as a separate software module. The created accelerator settings table will be loaded into the automated control program of the accelerator complex and sent to the control server of the accelerator complex according to the developed protocols, which will compare the data received from the built-in analog-to-digital converter (ADC), the channel of which will be allocated for an additional beam control module (it is possible to use the channel of the dose control system, since independent verification of the delivered dose in the visualization mode is not required). For the additional beam control module, it is planned to use thin scintillation films different from the standard ones and higher power supplies for the

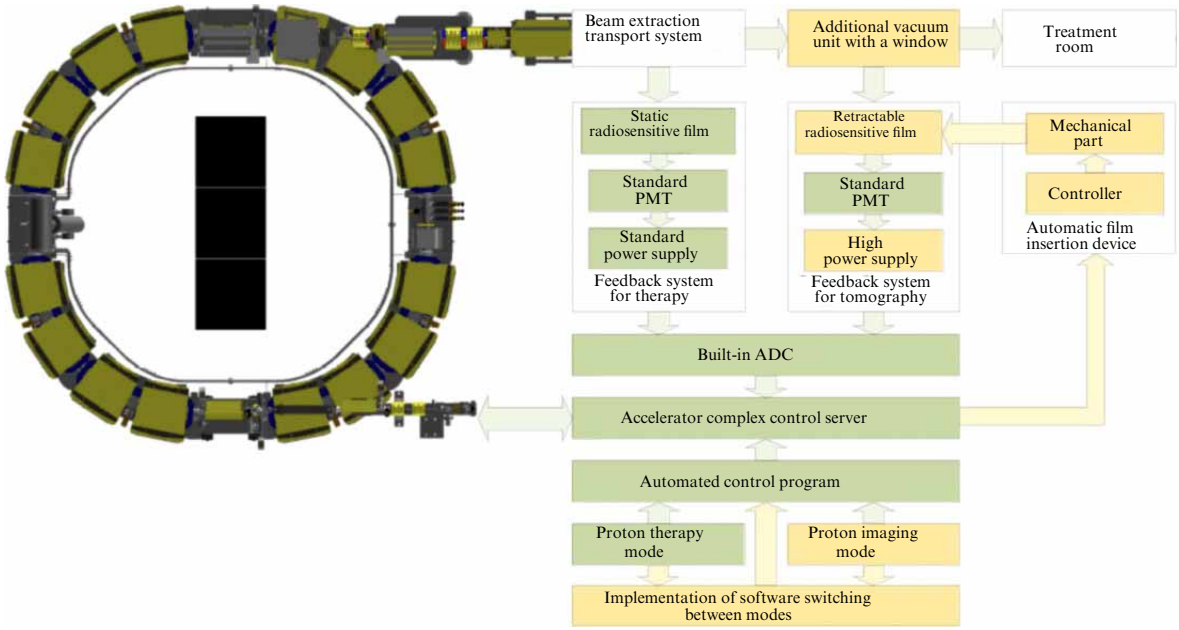

Figure 10. Schematic diagram of modernization of proton synchrotron of Lebedev Physical Institute for operation with the beam extraction mode for proton visualization.

PMT, while the PMT will be a standard one, namely a Hamamatsu R6094.

The accuracy of therapeutic procedures largely depends on preliminary diagnostics. Today, for oncological patients referred for PT, it is mandatory to undergo X-ray computed tomography before planning irradiation procedures. Then, the obtained Hounsfield units are converted into stopping powers of the medium for protons, which, in turn, are used by irradiation planning programs. Since photons and protons interact with matter differently, the use of X-ray data inevitably leads to uncertainties in the proton path lengths in biological tissues, as shown in Section 2.2. Even the most modern planning systems allow for an error estimated as $3.5\% + 1$ mm for the proton path lengths from the obtained X-ray data [70].

In Ref. [71], the requirements for the quality of an image obtained using a proton tomograph were formulated. The spatial resolution should be no worse than 1 mm, and the resolution in distinguishable tissue density, no less than 1%. The data collection time should be acceptable for clinical use, i.e., on average no more than 5 min (in some cases, no more than 10 min). The maximum dose for the entire scan should not exceed 5 cGy, since this value should be comparable to the same parameter of modern commercial X-ray imaging systems of the latest generations.

With the proper development of proton imaging and its large-scale implementation in clinical centers, the technology under consideration can significantly change the established standards of PT, making this method of treatment not only more accurate and safer for patients but also more accessible, since some of the procedures required today will lose their significance. However, despite the importance of proton imaging for the future development of PT and nuclear medicine in general, to date there is not a single implemented proton imaging system due to the lack of comprehensive solutions to the described problems, the unavailability of accelerator technologies, and the lack of reliable, proven algorithms for rapid reconstruction of proton images.

3. Binary technologies of proton therapy

Despite the effective use of proton therapy technologies across the globe, the problem of realizing the full potential of proton beams in clinical practice, including in the Prometheus proton therapy complex, has not been solved. Promising technologies aimed at increasing the effectiveness of proton therapy and minimizing the impact on healthy tissues include those based on binary nuclear-physical methods, such as the combined action of various ionizing radiation, as well as binary proton therapy technologies using nanosensitizers — chemical or pharmacological agents that increase the likelihood of cancer cell death during irradiation. In addition, an important area is the study of the possibility of fractionation, i.e., dividing the total radiation dose over time. The Prometheus proton therapy complex is regularly used to conduct studies of new scanning beam radiation therapy methods. New hypofractionation methods are being developed [72]. The effect of low and medium doses of protons on hematopoietic organs is being studied; in this case, these organs imitate healthy tissues of the patient during radiation therapy [73].

In binary technologies, targeting of the needed area is achieved by increasing the concentration, retention, and uniformity of distribution of the radiosensitizer [74–76]. Combined technologies based on the joint action of radiation and a pharmaceutical are already used in clinical practice. These include chemoradiotherapy [77], photodynamic therapy [76], neutron capture therapy [78–80], and other combined approaches [81].

The development of binary technologies based on the interaction of primary radiation and tumorotropic nanoparticles (NPs) functionalized for active targeting and visualization of tumors (nanoformulations) is considered an effective strategy for the treatment of malignant tumors [76]. (Targeted therapy is one that uses molecular-targeted drugs). When accumulated in a tumor, nanoparticles can localize and increase the dose directly in the pathogenic area, which

makes it possible to minimize radiation damage to healthy tissues. To maximize the effectiveness of this approach, it is necessary to take into account the specific effects leading to spatiotemporal heterogeneity of the radiosensitivity of normal and tumor cells, which are significantly enhanced by radiosensitizing nanoparticles. Binary technologies of radiation therapy using NPs suggest a significant expansion of the field of modern nuclear medicine due to integration with nanomedicine, which involves the use of NPs for cancer diagnosis and therapy, using their unique properties. The introduction of nonradioactive materials that can be activated from the outside using various external sources of nuclear particles to obtain radioactivity *in situ* is a new avenue for activating nanopreparations at the site of a cancer tumor, which can be considered *in situ* production of radiopharmaceuticals [82].

A task of primary importance for the implementation of the sensitization effect in proton therapy using nanoformulations is to determine the quantitative relationships among the properties of nanoparticles (material, shape and structure, coating and carriers), irradiation methods, and the biological effect that determines therapeutic efficacy. In 2018, the multidisciplinary scientific community NERT (Nanoparticle-Enhanced Radio Therapy) was organized [83]. The community includes scientists specializing in physics, chemistry, radiobiology, oncology, and nanotechnology. The main goal of the community is to use joint knowledge and developments for the clinical implementation and commercialization of NERT technologies, which will streamline the complex path from fundamental science to the clinic.

Sensitization of proton therapy with inorganic nanomaterials is a complex process that includes both the direct effect of the proton beam on DNA (single- and double-strand breaks) and cell organelles, and atomic interactions (generation of characteristic radiation, photoelectron cascades, Auger and Coster–Kronig electrons). Section 3 provides a review and analysis of literature data on the assessment of the possibilities and prospects for increasing the efficiency of PT using binary technologies and presents the results of research in the field of developing binary technologies using targeted nanoformulations, carried out using the Prometheus PTC. Two main approaches in binary PT technologies are considered: the use of nuclear reactions with the formation of particles with high linear energy transfer (LET) by introducing elements with a significantly larger radiation absorption cross section into the biological environment than that of the biological tissue itself, and the use of processes of interaction of protons and secondary track electrons with heavy metal nanoparticles ($Z > 52$) for PT sensitization.

3.1 Binary proton therapy using nuclear physical processes of proton interaction with boron nanoparticles

The main feature of nuclear reactions in PT is the possibility of generating particles with high LET, mainly α-particles. The main mechanism of α-particle generation is the excitation of tissue nuclei (O, C, N, H, Ca) during proton irradiation. The cross section of this process reaches hundreds of millibarns in a wide energy range. The resulting secondary short-range radiation with high LET can cause double-stranded DNA breaks, which in turn leads to the death of the pathogenic cell. This allows an increase in energy release in the pathogenic area and a pointwise increase in the absorbed dose in the target while reducing the relative dose absorbed in healthy tissues. In this case, the dose distribution is determined by the concentration distribution of the preparation injected into the tumor.

One striking example of this approach is the use of the boron-proton fusion reaction $p + {}^{11}B \rightarrow 3\alpha$ in proton therapy, when a boron-containing preparation is injected into the tumor. The reaction produces an excited compound nucleus ${}^{12}C^*$ which decays into an alpha particle and a beryllium ion ${}^{8}Be$, which then decays into two more alpha particles. The process is exothermic: when the lowest bound state of the system is reached after the emission of three alpha particles, a total energy of 8.7 MeV is released as kinetic energy transferred to the alpha particles. The expected energy of each particle is on average one third of the total, i.e., 2.9 MeV. However, the energy distribution range is wide and has an upper limit set by one alpha particle absorbing all the total energy and two others induced at rest [84]. The alpha particles that are products of the boron-proton fusion reaction have an average range in water of less than 30 μm, which is comparable to the typical size of a cell and determines the potential effectiveness of this method in therapy.

This approach underlies boron neutron capture therapy (BNCT) — a technology of selective destruction of malignant tumor cells by accumulating in them the stable isotope boron-10 and subsequent irradiation with epithermal neutrons [79, 80]. BNCT is a form of binary radiation therapy, which uses the uniquely high ability of the nonradioactive boron-10 nucleus to absorb a thermal neutron. The effective cross section of the neutron absorption reaction ${}^{10}B(n, \alpha)^7Li$ is 3835 bn for thermal neutrons and decreases inversely proportionally to the increase in neutron velocity. Absorption of a neutron by a boron nucleus leads to an instantaneous nuclear reaction with the release of energy of 2.79 MeV. In 6.1% of cases, the energy is distributed only between the lithium nucleus and the alpha particle; in 93.9% of cases, the lithium nucleus flies out in an excited state and emits a gamma quantum with an energy of 0.48 MeV.

However, despite the similarity of the approaches, the maximum value of the effective cross section of the $p + {}^{11}B \rightarrow 3\alpha$ nuclear reaction at a proton energy of 675 keV is only 0.9 bn. At low proton energies (0.1–5 MeV), the effective cross section of the reaction reaches a maximum, which increases the production of alpha particles near the Bragg peak region [85, 86]. This fact is one of the advantages of the potential use of the boron-proton fusion reaction in PT, which can reduce the energy of the primary proton beam and locally increase the dose directly in the tumor due to local energy release from secondary radiation.

Pioneering studies devoted to the potential effectiveness of boron use in PT have been carried out by a group of Korean researchers since 2014 [87–89]. The authors demonstrated the theoretical possibility of a sharp increase in the proton irradiation dose by introducing boron atoms into the irradiation area. However, the boron concentration values used in the studies (more than 10,000 ppm) are unattainable in practice. In 2016, gamma spectra induced by the $p + {}^{11}B \rightarrow 3\alpha$ reaction were experimentally detected [90]. The prompt gamma radiation emitted as a result of the boron-proton fusion reaction may be suitable for potential applications in gamma imaging.

In 2018, a group of Italian scientists experimentally studied for the first time the effectiveness of using a boron-containing preparation during proton irradiation *in vitro* and proved a decrease in the survival of cancer cells [91]. Sodium

borocaptate (BSH), used in BNCT, was used as a boron delivery agent [79]. The biological effects induced by the boron-proton reaction were investigated by measuring the death of clonogenic cells and chromosomal aberrations in a prostate cancer cell line (DU145) and a nonneoplastic breast epithelial cell line (MCF-10A). The cells were irradiated with a clinical proton beam of 62 MeV generated by a superconducting cyclotron (CATANA Eye PT Center, Institute of Nuclear Physics, Catania, Italy) in the presence of BSH. The working concentrations of ^{11}B were 80 and 40 ppm, which correspond to 0.17 and 0.08 mg ml^{-1} BSH, respectively. The clinical modified Bragg peak area was 30 mm in water and the cells were located at a depth of 24.86 mm in water equivalent, close to the middle of the SOBP (with an estimated LET value of $\sim$ 5 keV μm^{-1}). Fluorescence hybridization *in situ* staining techniques were used to evaluate the genotoxic effect of BSH. Dose–response curves for clonogenic survival were obtained at three positions along the SOBP, with and without BSH, demonstrating the absence of the BSH effect on cell death at the beam entrance. The dose change factors at the middle and distal ends of the SOBP were 1.4 and 1.75 $\pm$ 0.13, respectively. At this position, cell death is best described by a pure exponential for both proton irradiation alone and for proton irradiation in the presence of BSH. These experimental results, as well as the absence of a measurable effect of boron-11 at the beam entrance, where the incident beam energy is highest, in the authors' opinion, support the hypothesis of increased biological efficacy due to the occurrence of boron-proton fusion events. Proton irradiation resulted in higher numbers of all types of chromosomal aberrations in BSH-treated cells compared to cells irradiated with protons in the absence of BSH.

In 2021, the same group conducted an *in vitro* study using a 250-MeV proton beam used to treat deep-seated cancers at the National Center for Oncological Therapy (CNAO, Pavia, Italy) [92]. The authors used BSH as the ^{11}B carrier. The cell killing efficiency was assessed on DU145 prostate cancer cells, and chromosomal aberrations were quantified. Additionally, the authors assessed protein expression and DNA repair pathways using western blotting on noncancerous MCF-10A breast epithelial cells. The cells were irradiated at 3 positions: at the entrance, in the middle, and at the distal end of the modified Bragg peak. In addition, in the middle of SOBP, the authors examined the expression of DNA damage-activated repair proteins. The results of the study show that, in the distal position, BSH-treated samples had a higher yield of chromosomal aberrations than samples without the boron carrier during proton irradiation, whereas this was not observed at the beam entrance. A higher frequency of chromosomal aberrations was also observed at the distal region of SOBP compared to the previously obtained results at the middle position in BSH-treated MCF-10A cells.

In Ref. [93], the efficiency of using another boron-containing drug used in BRZT — boron phenylalanine (BPA) — was studied *in vitro* in a heterotopic model of glioblastoma. The authors found a significant increase in the therapeutic efficiency of proton irradiation in the presence of BPA, expressed in increased deaths of cancer cells and mitophagy. The results indicate a direct correlation between the presence of boron-containing BPA and cell apoptosis.

Thus, the results of studies [91–93] reliably showed an increase in therapeutic efficiency in the presence of boron-containing drugs in cancer cells during proton irradiation. The working hypothesis of the authors of the observed increase in therapeutic efficacy was that the boron-proton reaction results in the generation of short-range alpha particles with high LET, which damage DNA and kill cancer cells. It should be noted that there is an opposing point of view in the scientific community regarding the role of the boron-proton reaction and its effectiveness in providing the observed level of proton therapy sensitization. Thus, the calculated absorbed dose profiles along the proton track, obtained taking into account both all possible physical interactions of protons with the environment and only those from the interaction of protons with ^{11}B, show that the contribution to the total absorbed dose from the boron-proton fusion reaction in the case of a ^{11}B concentration of 80 μg g^{-1} is $\sim 10^{-7}$ [94]. This fact challenges the working hypothesis regarding the mechanism of cancer cell damage by alpha particles caused by the boron-proton fusion reaction. Furthermore, a recent study [95] demonstrated the absence of the radiosensitizing effect of BSH on glioma cells using proton beams with initial energies of 80 and 200 MeV. The authors found no significant effect of boron-11 concentrations up to 160 ppm on cell survival and colony formation. Moreover, for DU145 cells used in [91, 92], no significant effect was found when irradiating them at either the distal or proximal end of the Bragg peak, even when the boron-11 concentration was increased to 250 ppm.

In Ref. [96], the authors investigated the effect of ^{11}B compounds on clonogenic activity and the frequency of double-strand breaks in DU145 cancer cells irradiated with X-rays and protons. BSH and BPA were used as ^{11}B carriers at concentrations of 80 ppm of ^{11}B. In cells irradiated with protons with an average energy of 60.5 and 7.6 MeV near the Bragg peak, no effect of boron on the frequency of double-strand breaks was observed. The absence of changes in double-strand breaks means that the formation of alpha particles through the boron-proton fusion nuclear reaction has an insignificant effect on the biological effectiveness of proton irradiation, while the radiosensitizing effect of BSH is probably not associated with DNA damage. The minor radiosensitizing effect of BSH on DU145 cells did not depend on the proton energy and was also observed upon X-ray irradiation, which may be a consequence of the biochemical properties of the boron-containing compound [8, 97, 98].

To experimentally determine the efficiency of alpha particle generation in the $^{11}\mathrm{B} + \mathrm{p} \rightarrow 3\alpha$ nuclear reaction at the Lebedev Physical Institute [99], a study was conducted of the yield of the nuclear reaction near the proton resonance energy of 675 keV on the injector beam of the Prometheus proton synchrotron and a target made of natural boron. Alpha particles were recorded using a CR-39 track detector. During the experiment, the contribution to the overall statistics from defects on the detector surface (having sizes comparable to real tracks) and the contribution from protons that hit the detectors after scattering from the walls of the vacuum chamber were taken into account. For this purpose, the readings from the back sides of the detectors facing the chamber wall, which were located 10 cm from the target and approximately the same distance from the wall, were used. Figure 11 shows details of photographs of the detector surfaces, as well as histograms of the obtained areas of surface objects (tracks and various defects). The average flux of protons and alpha particles was obtained by subtracting the average 'background' from the results of processing each specific detector. The experimentally determined yield of

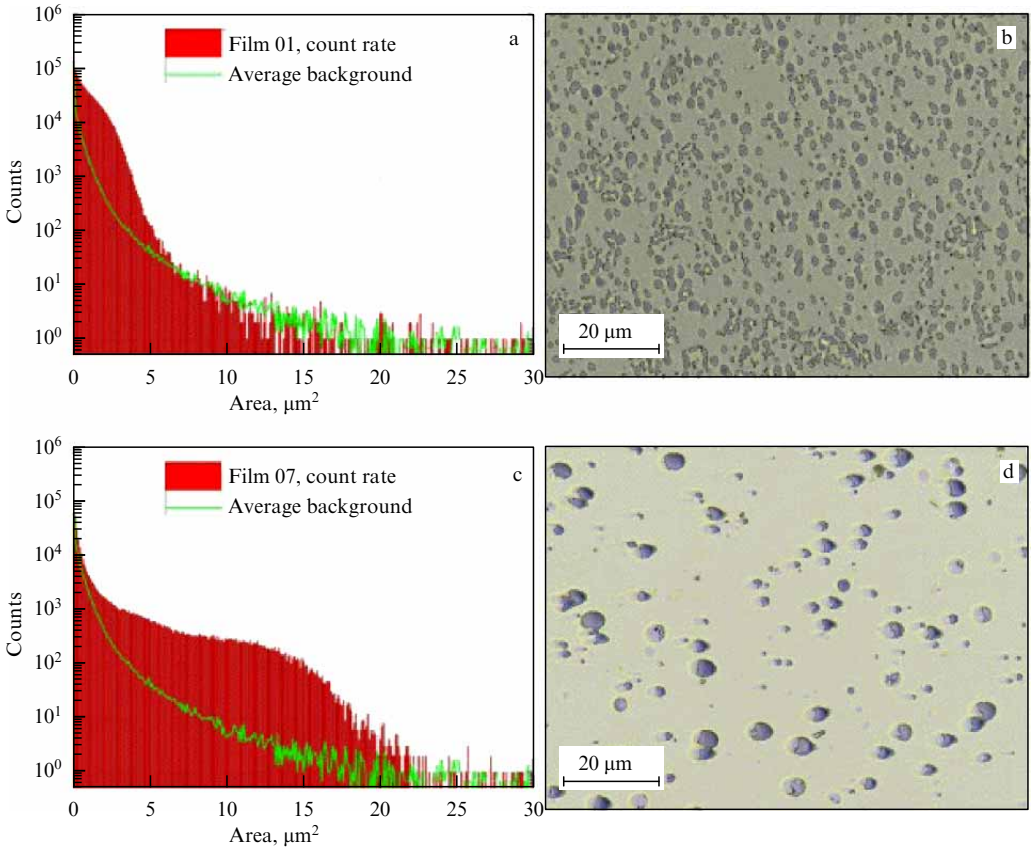

Figure 11. Details of microphotographs of detectors (b, d) and track area distribution (a, c) [99].

alpha particles near resonance was $\sim 10^{-4}$ alpha particles per proton. The estimated yield of alpha particles produced in the boron target per proton is significantly higher than the values obtained in [94] but is consistent with model calculations [100].

The use of elemental boron nanoparticles for sensitization of PTs was first demonstrated at the Lebedev Physical Institute using the Prometheus PTC [101]. Colloidal solutions of boron NPs were obtained by laser ablation methods in liquids; the NPs had an average size of 50 nm.

Laser ablation technologies in liquids have a proven high efficiency and ablation holds key advantages in terms of control of physical (low size dispersion with controlled average size) and physicochemical (chemical purity of the surface) parameters of the obtained nanomaterials and the production of nanoparticles for various types of therapy and visualization [102–107]. Particularly noteworthy is the use of laser synthesis of nanoparticles for nuclear and radiation medicine [108–110]. Laser ablation methods for the synthesis of nanoparticles for use in binary technologies have been optimized to produce colloidal solutions of NPs with the most suitable size fractions of these NPs for *in vivo* applications (from 7 to 55 nm) [111–114].

Subsequent functionalization of NPs with polyethylene glycol (PEG) ensured their biocompatibility and colloidal stability to increase their residence time in the bloodstream and thus maximize their accumulation in a tumor. Boron NPs were effectively taken up by human osteosarcoma MNNG/Hos cells and did not show significant toxic effects according to the results of the MTT test and clonogenic analysis.

The efficiency of boron NPs in the destruction of cancer cells under irradiation with a proton beam with an energy of 160.5 MeV was determined. Irradiation of MNNG/Hos cells at a dose of 3 Gy in the presence of boron NPs at concentrations of 80 and 100 ppm led to a decrease in the number of formed colonies of cells by 2 and 2.7 times, respectively, compared to the control samples irradiated in the absence of NPs (Fig. 12). It was found that irradiation with a proton beam in the presence of boron NPs leads to the formation of active oxygen species, which indicates the possible participation of a nonnuclear mechanism of cancer cell death associated with oxidative stress.

Thus, for the first time, using the Prometheus PTC, results were obtained indicating a significant increase in the efficiency of PT for oncological diseases due to the sensitization of the proton effect on the tumor in the presence of boron NPs.

3.2 Binary proton therapy using nanoparticles of heavy metals

The use of heavy metal nanoparticles as dose-enhancing agents in photon-capture therapy has demonstrated high therapeutic efficacy [115–119]. Clinical trials are being conducted with NPs based on three types of metals: PEG — gold nanoparticles, AGuIX — gadolinium polysiloxane nanoparticles, and NBTXR3 — hafnium oxide-based nanoparticles [8, 120, 121].

The first study on the efficacy of using metal NPs with proton irradiation was conducted in 2010 in *in vitro* and *in vivo* experiments, which demonstrated an increase in the antitumor efficacy of proton irradiation due to the introduction of iron and gold NPs [122]. This study, as well as its continuation [123], demonstrated the high therapeutic potential of using heavy metal NPs in PT. In Ref. [123], the effect of

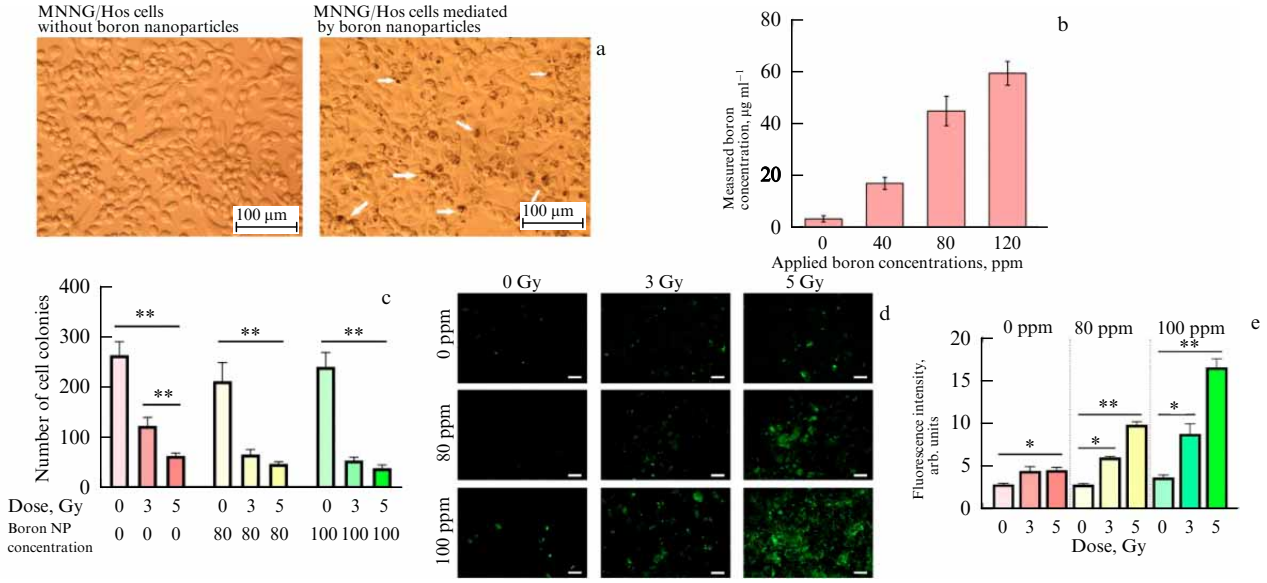

Figure 12. (a) Micrographs of MNNG/Hos osteosarcoma cells; arrows indicate nanoparticle aggregates on cell surface. (b) Quantitative analysis of boron concentration in cells by ICP-MS. (c) Clonogenic analysis of MNNG/Hos human osteosarcoma culture after incubation with boron NPs at different concentrations and their irradiation with a proton beam at the Bragg peak. (d) Photomicrographs of MNNG/Hos osteosarcoma cells after irradiation with a proton beam in the presence of boron NPs (80–100 nm). Scale bar — 100 μm. (e) Quantitative analysis of reactive oxygen species 24 h after irradiation with a proton beam in the presence of boron NPs using CellROX dye. $^{*}p \leqslant 0.05$; $^{**}p < 0.01$ using the Mann–Whitney U test.

14-nm iron NPs and 1.9-, 5-, and 14-nm gold nanoparticles was studied.

CT26 colon carcinoma was used as a tumor model, transplanted subcutaneously into the hind paw of Balb/C mice. Irradiation with a 45-MeV proton beam was performed with doses ranging from 10 to 100 Gy. Gold and iron nanoparticles were administered to mice intravenously at a concentration of 100 and 300 mg kg^{-1} by metal. The study was conducted for three variants of proton irradiation: in a modified Bragg peak geometrically covering the entire tumor volume, in a single unmodified Bragg peak located in the tumor volume, and with the Bragg peak located outside the tumor and the mouse body ('shoot-through' irradiation). For all doses and irradiation types, it was found that the introduction of nanoparticles leads to a more significant inhibition of tumor growth compared to control proton irradiation at the same dose, as well as to an increase in the number of complete tumor regressions. It was demonstrated that proton irradiation leads to complete tumor regression in 10–25% of animals (depending on the dose and type of irradiation), and the introduction of NPs makes it possible to increase the value of complete regression to 50–100%, depending on the size of the NPs, their concentration, and the irradiation dose. The dependence of the antitumor effect on the radiation dose and the concentration of the introduced nanoparticles was statistically reliable, which cannot be said about the dependence on the atomic number of the metal in the nanoparticle. It was found that both types of NPs cause the formation of a greater number of chemically active radicals than proton irradiation in the absence of nanoparticles, while iron NPs cause the formation of chemically active radicals twice as intensively as gold NPs do. It was also found that, in irradiated tumor tissues with metal nanoparticles in the area before the Bragg peak, the growth of this tumor is inhibited as effectively as with irradiation in the modified Bragg peak. Therefore, the use of metal nanoparticles to suppress micrometastases located outside the irradiation area and the modified Bragg peak seems promising. The results of an *in vitro* study on the DU145 prostate cancer cell line showed a decrease in cell survival from 18 to 42% when irradiated with 160-MeV protons in the modified Bragg peak area in the presence of gold NPs with a diameter of 44 nm attached to a transport platform made of the protein capsid of a bacteriophage [124]. Similar results were obtained in [125] when irradiating the epidermoid carcinoma cell line A431 with a 2-MeV proton beam in the presence of gold NPs with a diameter of 5 and 10 nm, functionalized with polyethylene glycol. It was found that irradiation of cells in the Bragg peak region in the presence of gold nanoparticles leads to a decrease in cell survival by 21–40%, depending on the irradiation dose.

At the Prometheus PTC, staff members of the Lebedev Physical Institute, the A F Tsyb Medical Research Center, and the National Research Nuclear University MEPhI conducted a series of studies to determine the most effective heavy metal nanoparticles and their use to increase the effectiveness of proton therapy due to their sensitizing effect. Using the laser ablation methods described above, gold nanoparticles [126], titanium nitride [127], bismuth (Bi) nanoparticles, and $(BiO)_2CO_3$ and $(BiO)_4CO_3(OH)_2$ nanosheets [128], Pd-Au nanoalloys [129] and Si-Au nanocomposites [130] were synthesized. The resulting nanoparticles were functionalized with biopolymers.

The greatest damaging effect *in vitro* upon proton irradiation of healthy and tumor cells of various lines in the presence of BiPluronic nanoformulations (NFs) (reduction in clonogenic activity by more than 90%) was detected in the Bragg peak region at NF concentrations of 50 μg ml^{-1} and a dose of 3 Gy.

Particular emphasis in the studies was placed on the targeted delivery of nanoformulations to the tumor area [131, 132]. Experiments were conducted on conjugation of the obtained Bi-Silane-PEG-COOH NF with targeted DARPin, Affibody molecules against HER2 and EpCAM mole-

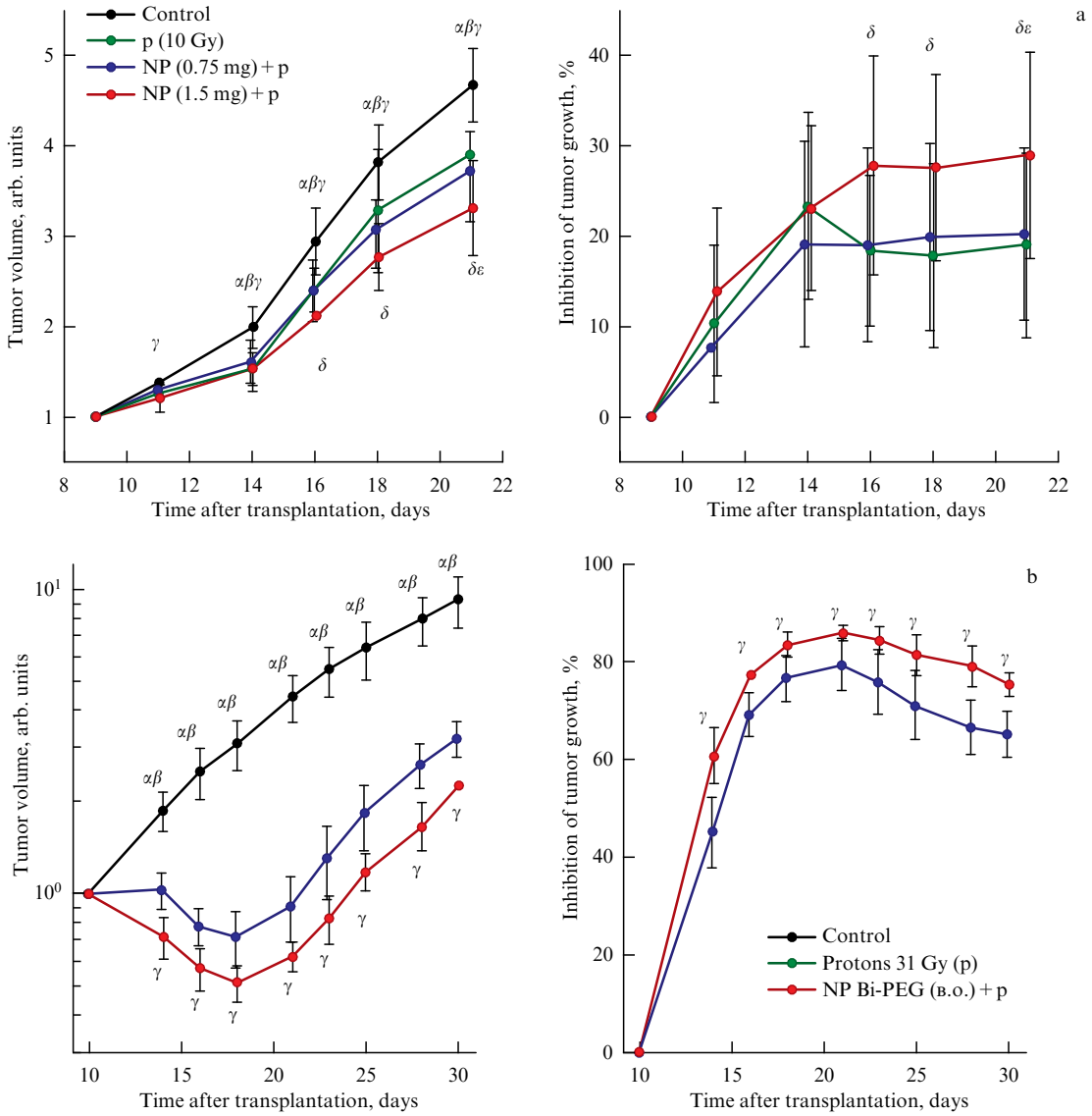

Figure 13. (a) Results of effect of local proton irradiation (10 Gy) alone and in combination with preliminary intratumoral administration of Bi-Pluronic NPs at doses of 0.75 and 1.5 mg on growth dynamics and growth inhibition of CEE. Graphic deviations correspond to SD. Symbols $\alpha, \beta, \gamma, \delta, \varepsilon$ — reliable differences between groups: α — control/protons; β — control/(NP 0.75 + protons); γ — control/(NP 1.5 + protons); δ — protons/(NP 1.5 + protons); ε — (NP 0.75 + protons)/(NP 1.5 + protons). (b) Effect of intratumoral administration of Bi-PEG-COOH NPs at a dose of 1.5 mg on antitumor effects of protons at a dose of 31 Gy against solid Ehrlich carcinoma in mice. Graphic deviations correspond to SD [133].

cules on the surface of cancer cells. The results of *in vivo* experiments on the study of tolerability, antitumor, and antimetastatic efficacy of different NPs and NFs and their effect on the efficacy of PT with intratumor and intravenous administration in transplantable tumor models are presented in Refs [133, 134]. It was found that Bi-PEG-COOH NFs with intratumor and intravenous administration can enhance the antitumor effect of PT; the achieved radiosensitizing effect was 15–20% and can be increased with an increase in the concentration of NPs and the dose of radiation exposure (Fig. 13).

In Ref. [134], the potential of using Au-PEG-FA nanoformulations based on gold nanoparticles and folic acid as a vector, aimed at the tumor folate receptor as PT sensitizers, was shown.

Nanoparticles caused complete inhibition of the clonogenic activity of EMT6/P adenocarcinoma *in vitro* at doses above 25 μg ml^{-1} and a radiation dose of 4 Gy. Preliminary results of therapy also showed significant additional slowing of tumor growth with binary exposure to NPs and protons. Binary therapy using gold NPs requires further study to determine in detail the biodistribution of particles and long-term effects of tumor treatment. The radiosensitizing effect is significant and stable: in the presence of Au-PEG-FA NPs, proton-induced growth inhibition of Ehrlich carcinoma significantly increases to 25%, while tumor growth inhibition reaches 80% (Fig. 14).

A study of the biodistribution of particles using computed tomography showed significant accumulation of targeted gold particles in the peritumoral stroma of the tumor nodule, where the largest number of living tumor cells is expected to be located [134]. These data demonstrate the efficacy of the folate conjugate as a tumor-specific vector for solid Ehrlich carcinoma.

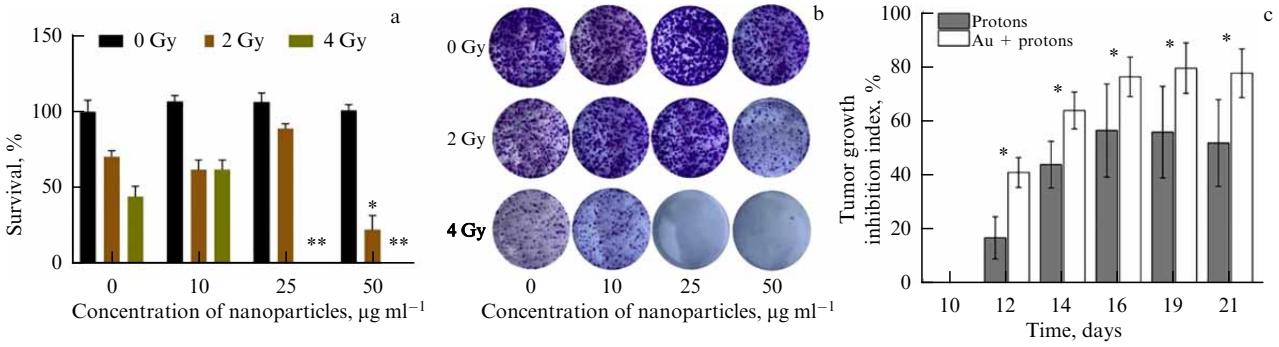

Figure 14. (a, b) Clonogenic analysis of EMT6/P adenocarcinoma cells after proton beam irradiation in the presence of Au-PEG nanoparticles; $^{**}p < 0.001$, $^{*}p < 0.05$, Student's t-test. (c) Growth inhibition indices of Ehrlich carcinoma *in vivo* after exposure to 31 Gy protons in the presence and absence of Au-PEG-FA nanoparticles, $^{*}p < 0.05$, Kruskal–Wallis test [134].

Thus, the use of nanoparticles in binary PT technologies is a promising way to increase the efficiency of radiation therapy for oncological diseases.

The question of the complex of processes underlying binary PT technologies and the mechanisms of PT sensitization in the presence of NPs and complexes based on them remains open. The mechanisms of interaction of nanoparticles with a proton beam include both physical processes of an additional increase in the absorbed dose due to secondary radiation, and chemical and biological processes leading to an increase in the radiosensitivity of the tumor. The diversity of emerging radiobiological effects leads to the fact that the efficiency of proton radiation sensitization is determined by a combination of several different NP characteristics and not only by the atomic number of the NP material, which is responsible for the cross section of atomic interaction processes. The results of the studies carried out with the Prometheus PTC [97, 129], as well as many other studies [82, 111, 114, 135–137], have shown that the antitumor efficiency correlates with the work function and the catalytic activity of the NP material. In particular, the results of a comparative *in vitro* analysis, as well as *in vitro* analysis of the efficiency of sensitization of proton therapy of NPs from materials with different work functions (WFs), namely gold (Au) ($Z = 79$, PB = 5.2 eV), bismuth (Bi) ($Z = 83$, PB = 4.3 eV), and boron-containing preparations (in particular, LaB_6, $Z = 57$, PB = 2.5 eV) have shown that the WF value of the NP material has a stronger effect on the efficiency of sensitization of proton exposure than its atomic number does. To achieve the same therapeutic effect (inhibition of tumor growth, change in the size of tumor nodes), the required concentration of LaB_6 (PB = 2.5 eV) in the target area was one tenth that for Au NPs (PB = 5.2 eV) and one fifth that for Bi NPs (PB = 4.3 eV). It should be noted that, despite the outstanding result in proton sensitization, LaB_6 NPs showed increased hepatotoxicity *in vivo*, which limits the potential for their clinical use. Complete biocompatibility of the NPs used in binary proton therapy is important.

3.3 Mathematical modeling of processes determining the efficiency of binary technologies of proton therapy

Before discussing the use of mathematical modeling methods to optimize binary PT technologies, it should be noted that mathematical modeling is primarily used in beam planning both to obtain a given dose distribution in the tumor and surrounding tissues and to reduce damage to normal tissue [138, 139]. Another important area in which mathematical modeling is actively used is the problem of spatiotemporal optimization of radiotherapy fractionation, including proton therapy [140–142]. Here, more attention is paid to the temporal optimization of fractionation protocols, but different approaches are used for this. The use of models expressed using ordinary differential equations is the most popular approach, including for describing binary technologies [143, 144]. This approach is attractive to mathematicians, since it often allows obtaining globally optimal solutions using analytical methods [145], but such models cannot consider 4-R radiobiology, and therefore are of little interest from a practical point of view.

Spatially distributed agent models allow these factors to be considered, but the computational complexity of such models leads to practical difficulties — it is impossible to use them to solve the problem of fractionation optimization with a realistic number of tumor cells, i.e., tumor size [146–148].

Only in recent years have studies appeared in which continuous spatially distributed mathematical models taking 4-R radiobiology into account are used to optimize radiotherapy [149].

Cell death during radiosensitization with nanoparticles is the result of complex physical, chemical, and biological effects caused by the combined effect of NPs and ionizing radiation. The radiosensitizing and synergistic effect of such nanoamplifiers is due to many physical, chemical, and biological factors, such as the atomic number (Z) of elements, the spectrum and dose of ionizing radiation, and the size, shape, structure, coating, functionalization, cellular localization, and concentration of the NPs [150]. Mathematical modeling of processes that determine the effectiveness of binary proton therapy technologies allows the optimization of binary proton therapy modes, as well as the parameters and properties of the NPs used.

In Ref. [151], the authors simulated a nanosphere of a given material surrounded by water using the TRAX Monte Carlo code. As a result, an increase in the proton dose of up to two times was observed for gold and platinum at a proton beam energy of 80 MeV. In Ref. [152], the authors simulated a single gold nanoparticle inside a water phantom and concluded that the production of secondary electrons increases with decreasing proton energy, while the average kinetic energy of secondary electrons arising from the interaction of a proton with a gold nanoparticle increases with increasing proton energy. In Ref. [153], a single gold NP in water was

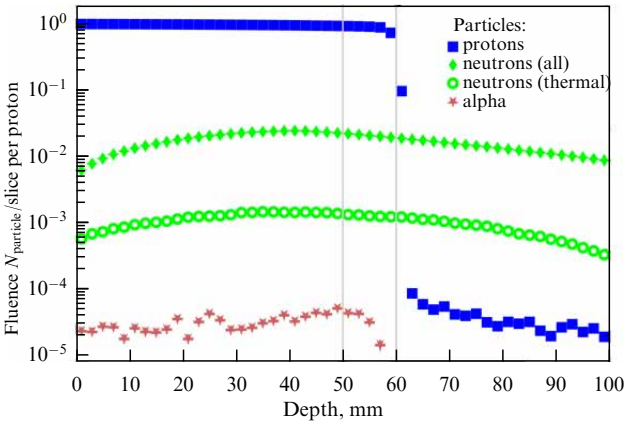

Figure 15. Fluence of protons, α-particles, thermal neutrons, and neutrons of all energies depending on depth in the tissue. Initial energy of proton beam is 87 MeV [156].

also simulated and the radial dose distribution due to secondary electrons was studied. It was found that the effect created by gold nanoparticles extends over several micrometers in the longitudinal direction and over several nanometers in the radial direction. In [154], the authors demonstrated the difference in the enhancement mechanisms between proton and photon interactions with NPs using Monte Carlo simulations. The biological model showed that protons require a higher concentration of gold nanoparticles to achieve the same effect as photons [155].

In [156], LPI researchers simulated nuclear reactions in the Geant 4.11 software environment using the QBBC model of interaction of radiation with matter. The simulated system was a cube 10 cm^3 in size, consisting of a tissue-like substance with a density $\rho = 0.986$ g cm^{-3} (oxygen (68%), carbon (18%), hydrogen (10%), nitrogen (3%)). The layer located at a depth of between 5 and 6 cm represented a malignant tumor. Radiosensitizing particles ^{10}B, ^{11}B, Au, Bi were introduced into it. The energy of the protons in the beam, $E = 87$ MeV, was selected so that the Bragg peak was located at the rear edge of the malignant layer. In this simulation, the concentration of radiosensitizers was set at 1000 mg l^{-1} (1000 ppm) in order to obtain statistically significant and unambiguous results. This is more than 10 times higher than the usual therapeutic values.

Figure 15 shows the particle flux densities depending on the depth in the tissue. It is evident that the flux density of the initial protons is almost completely preserved up to the Bragg peak. When protons interact with tissue nuclei, a significant number of fast neutrons are generated, some of which are slowed down to thermal energies (< 0.5 eV), where their capture cross sections for some nuclei increase by thousands of times. Of greatest interest is the production of α-particles due to their high LET.

Figure 16 shows the densities of α-particle and neutron production depending on the penetration depth into the tissue per beam proton. From Fig. 16a, it is evident that a noticeable number of α-particles are formed from the interaction of beam protons and tissue nuclei. It is important to note that the introduction of ^{10}B, ^{11}B, Au, Bi nanoparticles into the tumor does not result in a therapeutically significant increase in the production of α-particles. It follows from Fig. 16b that a significant number of neutrons are formed during the interaction of beam protons with tissue nuclei and radiosensitizers. Interaction with heavy elements, Au and Bi, leads to a significant increase in the production of fast neutrons in the tumor area.

Based on the results of the modeling, it can be concluded that the use of radiosensitizers in therapeutic concentrations does not provide a significant increase in the frequency of α-particle production. The obtained estimate of the α-particle yield for proton irradiation is 0.03 α-particles per cell with a size of 10 μm per Gy dose. For comparison, in neutron capture therapy using ^{10}B at a concentration of 30 ppm, a significant therapeutic effect is achieved at α-particle yield values almost two orders of magnitude higher (about 2.5 α-particles).

The experimentally observed effect of enhancing the action of proton irradiation with high-Z nanoparticles should be explained by other mechanisms, such as a change in the nature of radiochemical processes. Summarizing the results of the calculations, it is worth noting that the macroscopic effect of increasing the absorbed dose for realistic NP concentrations is very small. A physical boost and the occurrence of electron cascades cannot fully explain the observed effects [157, 158].

As an alternative to a direct increase in the dose during the interaction of proton radiation with metal nanoparticles, a mechanism of secondary electron emission due to surface plasmon excitation of nanoparticles was proposed in [159]. The authors showed that the interaction of 1 MeV protons with metal nanoparticles results in an order of magnitude greater emission of secondary electrons than because of direct

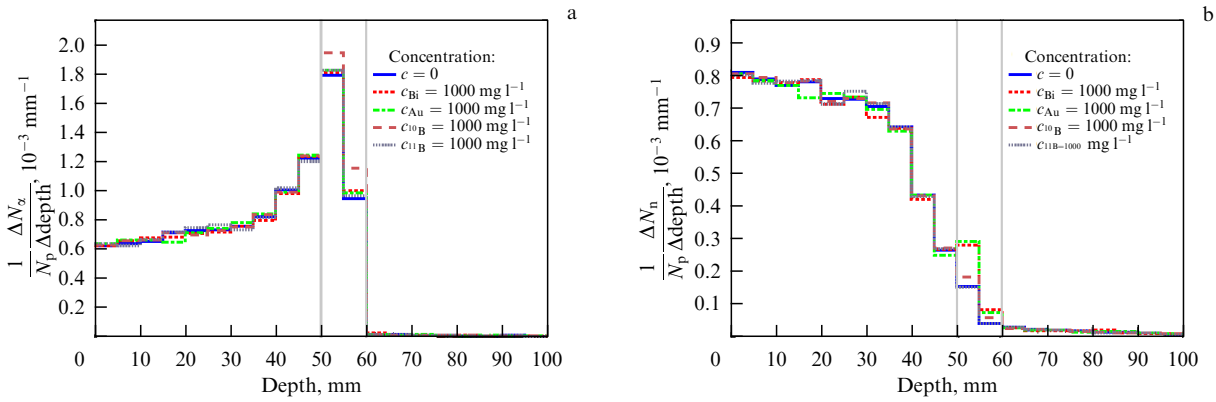

Figure 16. Production density of α-particles (a) and neutrons (b) depending on penetration depth into tissue per proton of a beam with an initial energy of 87 MeV [156].

ionization of NPs. In Ref. [160], the authors modeled radiation-induced radiochemical processes in the Geant4-DNA environment. Despite the underestimated number of emitted secondary electrons inherent in this model, the authors established the fact of increased water radiolysis and the formation of chemically active radicals due to the presence of gold nanoparticles, with the effect increasing with increasing proton energy. It should be noted that additional studies are needed, in particular to determine the true values of the cross sections of physical processes occurring during the interaction of protons with substances with a high atomic number Z; for example, the values of the cross sections of elastic and inelastic interaction of protons with such substances have not yet been determined with sufficient accuracy and significant discrepancies are observed, according to the ENDL nuclear data library [100].

Already in the middle of the 20th century, a linear-quadratic model,

$$\ln S = -\alpha D - \beta D^2,$$

began to be used for the mathematical description of the effect of radiotherapy on a tumor, where S is the proportion of surviving cells, D is the dose (equivalent) expressed in Grays (Gy), and α and β are the radiosensitivity parameters. This model has become classical, since it perfectly describes experimental data for doses not exceeding 5–6 Gy, and is actively used to this day to describe fractionated radiotherapy [161]. Cell death due to single-stage DNA double-strand breaks is considered to be characterized by the linear function (α), and the quadratic part of Eqn (β) describes the relationship of cell death with DNA strand breaks due to the accumulation of single-strand breaks. Most often, cancer cells have a higher α value than the surrounding normal tissues and a higher α/β ratio. As a result, the use of high doses can lead to serious side effects for normal tissue. To avoid such consequences, fractionation is used, when the total dose D is divided into N smaller doses $d = D/N$ and they are applied sequentially over a long period. The most common clinical fractionation protocols, developed on an empirical basis, use doses of 1.8–2 Gy delivered every weekday. In this case, the total dose depends on the histology, size, and location of the tumor, but, as a rule, lies in the range of 40–70 Gy.

In 1975, H R Withers introduced the concept of 4-R radiobiology to describe the main processes affecting the effectiveness of fractionated radiotherapy [162]. They include: *Repair* — reparation of nonlethal cellular damage, *Reoxygenation* — reoxygenation of the tumor and surrounding tissues, *Redistribution* — redistribution through the cell cycle, and *Repopulation* — repopulation of the tumor between irradiation fractions. Redistribution through the cell cycle implies that the radiosensitivity of a cell depends on its current position (phase) in the cell cycle. At least in part, this is due to conformational changes in DNA, which affect the complexity and, therefore, the success of the repair processes [163]. In particular, nonproliferating or immobile cells are more radioresistant. Tumor reoxygenation is important, since cells are more radiosensitive in the presence of oxygen. This effect only occurs if oxygen is present either during irradiation or immediately after a few milliseconds and is usually explained by the oxygen fixation hypothesis [164].

Depending on the type of radiotherapy used, these effects have different significance. Thus, radiotherapy using carbon ions with a significantly higher α/β ratio than photon therapy is practically insensitive to reoxygenation. In this sense, PT is in an intermediate state — its effectiveness depends on the oxygen level in much the same way as photon therapy, but at the same time it has a higher α/β ratio and therefore a higher proportion of double-strand DNA breaks. All this must be taken into account when talking about the search for optimal regimens of PT fractionation or its use together with radiosensitizing nanoformulations in the framework of binary therapy.

In binary therapy using radiosensitizing preparations, another task is to predict the distribution of the radiosensitizer after its introduction into the bloodstream. There are a limited number of studies in this area [165, 166]. It should be noted that these papers do not analyze the antitumor effect of the preparation, and the model itself in most cases either does not take into account the process of tumor angiogenesis or considers it in a simplified version.

Discussing radiosensitization using tumor-specific nanoparticles, each of which is an active substance coated with a polymer layer with antibodies embedded in it, we face an additional problem of determining the optimal size of nanoparticles, the solution to which is possible using mathematical modeling methods. A contradiction arises between the need to have the maximum amount of sensitizer in a particle, which encourages an increase in its size, and the need to ensure the transport of NPs to the tumor, but this is hindered by factors such as: the location of newly formed tumor capillaries, for the most part not deep in the tumor but at its border with normal tissue [167]; the need to penetrate through pores in capillary walls of limited size [168]; and increased pressure of the intercellular fluid in the tumor [169]. A study of this issue using mathematical modeling methods [170] showed that the optimal size of nanoparticles is in the region of 30 nm (Fig. 17), which is in good agreement with experimental data on the effect of increased permeability and retention of high-molecular compounds in the tumor [171].

Thus, in mathematical modeling of binary PT technologies, it is necessary to take into account both the characteristics of the radiobiological effect on tumor and normal tissue, and the transport of the nanosensitizer to the tumor [172].

4. Prospective technologies of proton therapy and modernization of Prometheus proton therapy complex

An obvious avenue for the development of the Prometheus complex is the above-mentioned possibility of PT of a wide range of oncological diseases (breast cancer, lung cancer, prostate cancer, etc.) using proton irradiation of malignant tumors of various localizations with the patient in a lying position.

When using the scanning proton beam of the Prometheus PTC to localize a tumor in patients irradiated in a lying position, there is a shortage of angles for delivering the beam to the tumor. Dynamic gantry systems, widely used in imported proton accelerators, are now considered excessively complex and expensive, and more and more PT centers are turning their attention to systems with a fixed beam. It is proposed to solve the shortage of irradiation angles by adding an additional beam output at an angle to the patient (Fig. 18).

It is envisaged to modernize the Prometheus PTC by developing and implementing a system for an additional fixed proton beam output at an angle to the patient in a

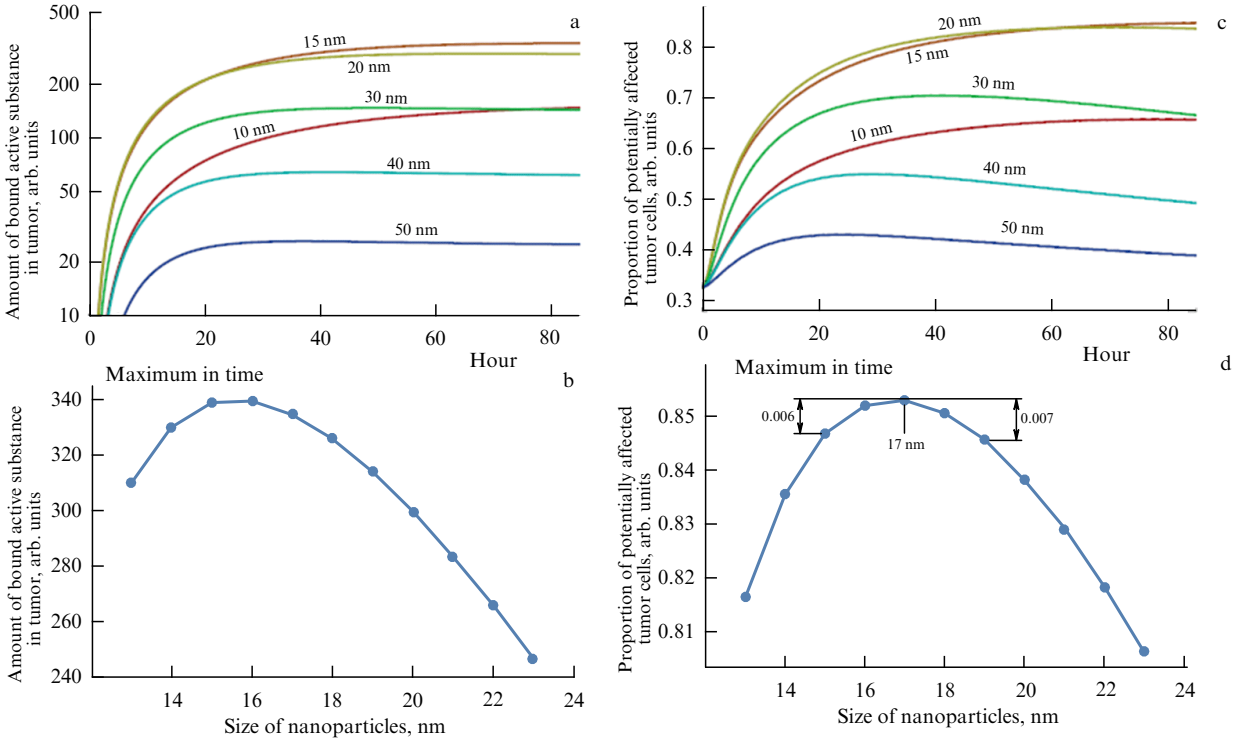

Figure 17. Dynamics of bound sensitizing substance (a, b) and proportion of potentially affected tumor cells (c, d) upon administration of a specific nanosensitizer of different radii with a uniform spectrum of pores of abnormal capillaries in range of 1–100 nm. In Figures a, b, the concentration of preparation in the blood at the time of administration is taken as a unit along ordinate axis.

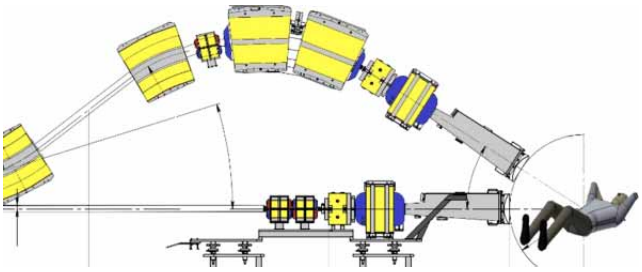

Figure 18. Scheme of additional beam output at an angle to the patient.

prone position. Additional angles will significantly reduce the dose load on healthy tissues and expand the scope of application of the Prometheus PTC. It is assumed that the additional channel will have a system of focusing lenses similar to the main one, magnets for fast horizontal and vertical beam scanning, as well as a system for controlling the intensity and coordinates of the beam. This will ensure consistent irradiation of targets within one fraction at different angles without wasting time on rotating the beam transport system. Unlike the rotating gantry system, fixed beam delivery channels are easy to operate, since they do not require daily checking of rotation accuracy, do not wear out over time, and do not require large rooms for installation. It is important to note that the additional release channel is easy to operate and will not lead to a significant increase in the cost or the dimensions of the complex.

Verification of patients in a lying position also raises the task of developing a patient positioning system using two orthogonal X-ray beams with the subsequent possibility of replicating this technology in other radiation therapy centers. A new system for verifying the position of an object based on

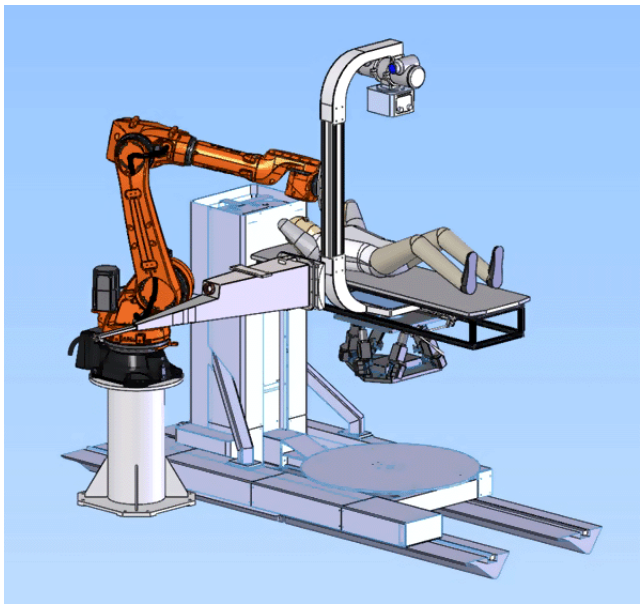

Figure 19. Illustration of a system for verifying the position of an object based on a high-power X-ray source and a detection screen mounted on a robotic manipulator.

a high-power X-ray source and a detecting screen attached to a robotic manipulator will complement the Prometheus PTC (Fig. 19). High power in the X-ray source will provide high-quality images of large objects. This technology will create a high-precision system for monitoring the position of an object in space. An important feature of such a design will be the universality of its use for the patient both in the lying and in the sitting position.

5. Conclusion

The review analyzes the results of solving new fundamental problems and major applied developments in the field of applying nuclear physics methods for creating new technologies for diagnostics and proton therapy of socially significant diseases using the proton synchrotron of the Lebedev Physical Institute and the Prometheus proton therapy complex developed on its basis. The article presents the results of developing new binary nuclear physics methods using promising nanoparticles and systems based on them as therapy stabilizers aimed at creating targeted therapy methods. The introduction of nonradioactive nanoparticles to obtain radioactivity *in situ* upon external activation using various external sources is one of the newest areas in the treatment of malignant tumors, which can be considered *in situ* production of 'nanoradiopharmaceuticals.' The prospects for the development of proton radiography (visualization) using the maximum energy of protons are shown. The developed technologies of proton therapy with a scanning beam, taking into account the movement of the tumor, expand the list of tumor localizations in hard-to-reach places (lungs, chest, etc.). Improvement and modernization of the Prometheus PTC involves the possibility of modernizing the complex and introducing the developed proton therapy technologies.

Acknowledgments. The authors express their deep gratitude to Vladimir Egorovich Balakin for the conceptual basis that he laid in the direction of development of nuclear physics methods and proton therapy technologies. The authors express their gratitude and appreciation to all colleagues and co-executors of the project Development of New Technologies for Diagnostics and Radiation Therapy of Socially Significant Diseases with Proton and Ion Beams Using Binary Nuclear Physics Methods, implemented at the Lebedev Physical Institute jointly with the National Medical Research Center of Radiology of the Ministry of Health of the Russian Federation and the National Research Nuclear University MEPhI within the framework of the Federal Scientific and Technical Program for the Development of Synchrotron and Neutron Research for 2019–2027 with the support of the Ministry of Education and Science of the Russian Federation, including A V Kabashin, A A Popov (National Research Nuclear University MEPhI); S M Deev, P A Kotelnikova (Institute of Bioorganic Chemistry, Russian Academy of Sciences); A L Popov (Institute of Theoretical and Experimental Biophysics, Russian Academy of Sciences); A I Bazhan, A E Shemyakov, M A Belikhin (Physics and Technology Center, Lebedev Physical Institute); S N Koryakin, M V Filimonova (A F Tsyb Medical Radiological Research Center), as well as employees of JSC Protom for providing the materials used in the manuscript, and D S Petruna for invaluable assistance in preparing the manuscript. The work was supported by the Ministry of Science and Higher Education of the Russian Federation, grant no. 075-15-2021-1347.

References

1. Klenov G I, Khoroshkov V S *Phys. Usp.* **59** 807 (2016); *Usp. Fiz. Nauk* **186** 891 (2016)
2. Durante M, Galès S (Conveners), in *Nuclear Physics for Medicine* (Eds F Azaiez et al.) (European Science Foundation, Nuclear Physics European Collaboration Committee — NuPECC, 2014) p. 11
3. Krasavin E A *Phys. Usp.* **59** 411 (2016); *Usp. Fiz. Nauk* **186** 435 (2016)
4. Paganetti H *Proton Beam Therapy* (Bristol: IOP Publ., 2017)
5. Chernyaev A P, Lykova E V *Phys. Part. Nucl. Lett.* **20** 729 (2023); *Pis'ma Fiz. Elem. Chast. At. Yad.* **20** 753 (2023)
6. Thun M J et al. *Carcinogenesis* **31** 100 (2010)
7. World Health Organization, https://www.who.int/health-topics/cancer
8. Kaprin A D, Starinskii V V, Shakhzadova A O (Ed.) *Zlokachestvennye Novoobrazovaniya v Rossii v 2022 g.* (Malignant Neoplasms in Russia in 2022) (Moscow: MNIOI im. P.A. Gertsena — Filial FGBU NMITs Radiologii Minzdrava Rossii, 2023)
9. Bragg W H, Kleeman R *Phil. Mag.* **8** 726 (1904)
10. "Proton and Photon Consortium Registry (PPCR): A Multi Center Registry of Pediatric Patients Treated With Radiation Therapy," NCT01696721, https://www.clinicaltrials.gov/study/NCT01696721
11. Durante M, Orecchia R, Loeffler J S *Nat. Rev. Clin. Oncol.* **14** 483 (2017)
12. Loeffler J S, Durante M *Nat. Rev. Clin. Oncol.* **10** 411 (2013)
13. Durante M, Loeffler J S *Nat. Rev. Clin. Oncol.* **7** 37 (2010)
14. The Particle Therapy Co-Operative Group (PTCOG), https://ptcog.site
15. Chernyaev A P et al. *Med. Radiol. Rad. Bezopasn.* **64** (2) 11 (2019) https://doi.org/10.12737/article_5ca5a0173e4963.18268254
16. Ivanov E M et al. *Med. Radiol. Rad. Bezopasn.* **67** (3) 41 (2022) https://doi.org/10.33266/1024-6177-2022-67-3-41-46
17. Dzhelepov V P et al. *IEEE Trans. Nucl. Sci.* **20** 268 (1973)
18. Dzhelepov V P, Komarov V I, Savchenko O V *Med. Radiol.* **14** (4) 54 (1969)
19. Granov A M et al. *Med. Fiz.* (2) 10 (2016)
20. Balakin V E et al., in *26th Russian Particle Accelerator Conf., RUPAC'18, Protvino, Russia, 1–5 October 2018* (Protvino: JACoW, 2018) p. 135
21. Pryanichnikov A A, Sokunov V V, Shemyakov A E *Phys. Part. Nucl. Lett.* **15** 981 (2018); *Pis'ma Fiz. Elem. Chast. At. Yad.* **15** 993 (2018)
22. Ulyanenko S E et al. *Issled. Praktika Meditsine* **4** (S1) 107 (2017)
23. Smyk D I et al. *Opukholi Golovy Shei* **12** (4) 39 (2022) https://doi.org/10.17650/2222-1468-2022-12-4-39-47
24. Gordon K et al. *Radiation Oncology* **16** 238 (2021) https://doi.org/10.1186/s13014-021-01961-9
25. Gulidov I et al. *JBUON* **26** 970 (2021)
26. Gordon K et al. *Rep. Pract. Oncol. Radiother.* **26** (2) 203 (2021)
27. Dr. Sergey Berezin Medical Institute (MIBS), Proton Therapy Center, https://protherapy.ru/
28. Shulepova L I et al. *Med. Fiz.* (3) 43 (2019)
29. Strekopytov V "Tselebnaya moshch' uskoritelya. Sozdan metod mgnovennogo izlecheniya ot raka" ("The healing power of the accelerator. A method for instant cure of cancer has been created"), RIA News, 30.11.2022, https://ria.ru/20221130/ultraflesh-1835099370.html
30. Balakin V E et al., in *The 2nd Intern. Symp. on Physics, Engineering and Technologies for Biomedicine* (KnE Energy & Physics, 2018) p. 45, https://doi.org/10.18502/ken.v3i2.1790
31. Volz L et al. *Front. Oncol.* **12** 930850 (2022)
32. Buchner T et al., in *8th IEEE RAS/EMBS Intern. Conf. for Biomedical Robotics and Biomechatronics, BioRob, 29 November–01 December 2020, New York, NY, USA* (Piscataway, NJ: IEEE, 2020) p. 981, https://doi.org/10.1109/BioRob49111.2020.9224389
33. Hegarty S et al. *Front. Oncol.* **12** 821887 (2022)
34. Rahim S et al. *Front. Oncol.* **10** 213 (2020)
35. Yan S et al. *Int. J. Radiat. Oncol. Biol. Phys.* **95** 224 (2016)
36. Schreuder A N et al. *J. Appl. Clin. Med. Phys.* **24** e14099 (2023)
37. Lebedeva Zh S, Shurakova Yu B *Nauch.-Tekh. Vedomosti St. Peterburg. Politekh. Univ. Fiz.-Mat. Nauki* (4(182) Pt. 1) 66 (2013)
38. Kubiak T *Br. J. Radiol.* **89** 20150275 (2016)
39. Trnková P et al. *Phys. Medica Eur. J. Med. Phys.* **54** 121 (2018)
40. Bertholet J et al. *Phys. Med. Biol.* **64** 15TR01 (2019)
41. Han Y *Radiat. Oncol. J.* **37** (4) 232 (2019)
42. Wang N et al. *Radiat. Oncol.* **8** 73 (2013)
43. Li Y R, Kirk M, Lin L *Int. J. Part. Therapy* **3** 320 (2016)
44. Dolde K et al. *Phys. Med. Biol.* **64** 085011 (2019)

45. Mizuhata M et al. *Cancers* **10** (2) 58 (2018)
46. Bert C, Rietzel E *Radiat. Oncol.* **2** 24 (2007)
47. Bert C, Herfarth K *Radiat. Oncol. J.* **12** 170 (2017)
48. Eley J G et al. *Phys. Med. Biol.* **59** 3431 (2014)
49. Bert C et al. *Technol. Cancer Res. Treat.* **13** 485 (2014)
50. Shimizu S et al. *PLoS ONE* **9** e100425 (2014)
51. "Spearheading global fight against cancer with proton therapy," Hokkaido Univ., https://www.global.hokudai.ac.jp/blog/tgi02-spearheading-global-fight-against-cancer-with-proton-therapy
52. Kohli K et al. *BioMed. Eng. OnLine* **13** 144 (2014) https://doi.org/10.1186/1475-925X-13-144
53. Belikhin M A et al. *Bull. Lebedev Phys. Inst.* **49** 132 (2022); *Kratk. Soobshch. Fiz. FIAN* (5) 22 (2022)
54. Schneider U, Pedroni E *Med. Phys.* **22** 353 (1995)
55. Penfold S N et al. *Med. Phys.* **36** 4511 (2009)
56. Hanson K M et al. *IEEE Trans. Nucl. Sci.* **25** 657 (1978)
57. Hanson K M *IEEE Trans. Nucl. Sci.* **26** 1635 (1979)
58. Hanson K M et al. *Phys. Med. Biol.* **26** 965 (1981)
59. Hanson K M et al. *Phys. Med. Biol.* **27** 25 (1982)
60. Miller C et al. *J. Radiat. Oncol.* **8** 97 (2019)
61. Pryanichnikov A A, Chernyaev A P, Khoroshkov V S *Vvedenie v Fiziku i Tekhniku Protonnoi Terapii* (Introduction to the Physics and Technique of Proton Therapy) (Moscow: Fizicheskii Fakul'tet MGU, 2019)
62. Esposito M et al. *Phys. Medica Eur. J. Med. Phys.* **55** 149 (2018)
63. DeJongh E A et al. *Med. Phys.* **48** 1356 (2021)
64. Amaldi U et al. *Nucl. Instrum. Meth. Phys. Res. A* **629** 337 (2011)
65. Bashkirov V A et al. *Med. Phys.* **43** 664 (2016)
66. Shemyakov A E et al. *Phys. Medica Eur. J. Med. Phys.* **94** S119 (2022)
67. Pryanichnikov A et al. *Phys. Medica Eur. J. Med. Phys.* **94** S113 (2022)
68. Zavestovskaya I N et al. *Bull. Lebedev Phys. Inst.* **49** 145 (2022); *Kratk. Soobshch. Fiz. FIAN* (5) 41 (2022)
69. Pryanichnikov A A et al. *Moscow Univ. Phys. Bull.* **77** 657 (2022); *Vestn. Mosk. Univ. Ser. 3. Fiz. Astron.* (4) 59 (2022)
70. Schultze B et al. *IEEE Access* **9** 25946 (2021)
71. Schulte R et al. *IEEE Trans. Nucl. Sci.* **51** 866 (2004)
72. Balakin V E et al. *Biophysics* **61** 682 (2016); *Biofizika* **61** 866 (2004)
73. Balakin V E et al. *Dokl. Biochem. Biophys.* **494** 231 (2020); *Dokl. Ross. Akad. Nauk. Nauki Zhizni* **494** 458 (2020)
74. Sheino I N et al. *Byull. Sibir. Med.* **16** (3) 192 (2017)
75. Kulakov V N et al. *Pharm. Chem. J.* **50** 388 (2016)
76. Bushmanov A Yu et al. *Med. Radiol. Rad. Bezopasn.* **64** (3) 11 (2019)
77. Seiwert T Y, Salama J K, Vokes E E *Nat. Clin. Pract. Oncol.* **4** 86 (2007)
78. Connell P P, Hellman S *Cancer Res.* **69** (2) 383 (2009)
79. Sauerwein W, Wittig A, Moss R, Nakagawa Y (Eds) *Neutron Capture Therapy. Principles and Applications* (Heidelberg: Springer, 2012)
80. Zavestovskaya I N et al. *Int. J. Mol. Sci.* **24** 17088 (2023)
81. Bergs J W J et al. *Biochim. Biophys. Acta BBA Rev. Cancer* **1856** 130 (2015)
82. Roy I et al. *ACS Nano* **16** 5036 (2022)
83. Ricketts K et al. *Br. J. Radiol.* **91** 20180325 (2018)
84. Ruggiero A G, in *Contribution to Conf. on Prospects for Heavy Ion Inertial Fusion, Aghia Pelaghia, Crete, Greece, September 26 – October 1, 1992*, pp. 1 – 19
85. Becker H W, Rolfs C, Trautvetter H P *Z. Phys. A* **327** 341 (1987)
86. Segel R E, Hanna S S, Allas R G *Phys. Rev.* **139** B818 (1965)
87. Yoon D-K, Jung J-Y, Suh T S *Appl. Phys. Lett.* **105** 223507 (2014)
88. Jung J-Y et al. *AIP Advances* **6** 095119 (2016)
89. Jung J-Y et al. *Oncotarget* **8** 39774 (2017)
90. Petringa G et al. *JINST* **12** C03059 (2017)
91. Cirrone G A P et al. *Sci. Rep.* **8** 1141 (2018)
92. Bláha P et al. *Front. Oncol.* **11** 682647 (2021)
93. Cammarata F P et al. *Commun. Biol.* **6** 388 (2023)
94. Mazzone A et al. *Eur. Phys. J. Plus* **134** 361 (2019)
95. Shtam T et al. *Sci. Rep.* **13** 1341 (2023)
96. Manandhar M et al. *Med. Phys.* **49** 6098 (2022)
97. Koldaeva E Yu et al., in *New Challenges in Neutron Capture Therapy 2010. Proc. of the 14th Intern. Congress on Neutron Capture Therapy, Buenos Aires, 2010*, p. 144
98. Lebedev D et al. *RAD Conf. Proc.* **4** 60 (2020) https://doi.org/10.21175/RadProc.2020.12
99. Zavestovskaya I N et al. *Bull. Lebedev Phys. Inst.* **50** 279 (2023); *Kratk. Soobshch. Fiz. FIAN* (7) 22 (2023)
100. Bagulya A V et al. *Bull. Lebedev Phys. Inst.* **50** 138 (2023); *Kratk. Soobshch. Fiz. FIAN* (4) 27 (2023)
101. Zavestovskaya I N et al. *Nanomaterials* **13** 2167 (2023)
102. Maximova K et al. *Nanotechnology* **26** 065601 (2015)
103. Afanasiev Y V et al. *Appl. Phys. A* **64** 561 (1997)
104. Kabashin A et al. *Sci. Rep.* **6** 4732 (2016)
105. Kharin A Yu et al. *Adv. Opt. Mater.* **7** 1801728 (2019)
106. Oleshchenko V A et al. *Appl. Surf. Sci.* **516** 145661 (2020)
107. Zavestovskaya I N *Quantum Electron.* **40** 942 (2010); *Kvantovaya Elektron.* **40** 942 (2010)
108. Kabashin A V et al. *ACS Nano* **13** 9841 (2019)
109. Popova-Kuznetsova E et al. *Nanomaterials* **10** (1) 69 (2020)
110. Petriev V M et al. *Sci. Rep.* **9** 2017 (2019)
111. Belyaev I B et al. *Bull. Lebedev Phys. Inst.* **49** 185 (2022); *Kratk. Soobshch. Fiz. FIAN* (6) 55 (2022)
112. Zelepukin I V et al. *J. Control. Release* **349** 475 (2022)
113. Pastukhov A I et al. *Sci. Rep.* **12** 9129 (2022)
114. Tikhonowski G V et al. *Bull. Lebedev Phys. Inst.* **49** 180 (2022); *Kratk. Soobshch. Fiz. FIAN* (6) 47 (2022)
115. Chithrani D B et al. *Radiat. Res.* **173** 719 (2010)
116. Lechtman E et al. *Phys. Med. Biol.* **58** 3075 (2013)
117. Taupin F et al. *Phys. Med. Biol.* **60** 4449 (2015)
118. Bonvalot S et al. *Clinic. Cancer Res.* **23** 908 (2017)
119. Hainfeld J F et al. *Phys. Med. Biol.* **49** N309 (2004)
120. Libutti S K et al. *Clinic. Cancer Res.* **16** 6139 (2010)
121. Lux F et al. *Br. J. Radiol.* **92** 1093 20180365 (2019)
122. Kim J-K et al. *Nanotechnology* **21** 425102 (2010)
123. Kim J-K et al. *Phys. Med. Biol.* **57** 8309 (2012)
124. Polf J C et al. *Appl. Phys. Lett.* **98** 193702 (2011)
125. Li S et al. *Nanotechnology* **27** 455101 (2016)
126. Bailly A et al. *Sci. Rep.* **9** 12890 (2019)
127. Popov A A et al. *Sci. Rep.* **9** 1194 (2019)
128. Bulmahn J C et al. *Nanomaterials* **10** 1463 (2020)
129. Holade Y et al. *Catal. Sci. Eng.* **10** 7955 (2020)
130. Al-Kattan A et al. *Nanomaterials* **11** 592 (2021)
131. Shipunova V O et al. *ACS Appl. Mater. Interfac.* **10** 17437 (2018)
132. Aghayeva U F et al. *ACS Nano* **7** 950 (2013)
133. Filimonova M V et al. *Byull. Eksp. Biol. Med.* **176** (11) 647 (2023)
134. Filimonova M V et al. *Dokl. Ross. Akad. Nauk. Nauki Zhizni* accepted for publication 29.02.2024
135. Zelepukin I V et al. *J. Control. Release* **349** 475 (2022)
136. Savinov M S et al. *Bull. Lebedev Phys. Inst.* **50** S1265 (2023); Translated from Russian: *Kvantovaya Elektron.* **53** 575 (2023)
137. Skribitskaya A V et al. *Bull. Lebedev Phys. Inst.* **50** S1272 (2023) https://doi.org/10.3103/S1068335623220153; Translated from Russian: *Kvantovaya Elektron.* **53** 580 (2023)
138. Souris K et al. *Med. Phys.* **46** 4676 (2019)
139. Pryanichnikov A A et al. *Phys. Part. Nucl. Lett.* **17** 629 (2020); *Pis'ma Fiz. Elem. Chast. At. Yad.* **17** 707 (2020)
140. Gaddy M R et al. *Phys. Med. Biol.* **63** 015036 (2018)
141. Kuznetsov M B, Kolobov A V *Bull. Lebedev Phys. Inst.* **49** 174 (2022); *Kratk. Soobshch. Fiz. FIAN* (6) 37 (2022)
142. Unkelbach J, Paganetti H *Seminars Radiat. Oncol.* **28** (2) 88 (2018)
143. Badri H et al. *J. Math. Biol.* **72** 1301 (2016)
144. Kovalenko S Yu, Yusubalieva G M *Komp'yut. Issled. Model.* **10** (1) 113 (2018)
145. Bertuzzi A et al. *J. Math. Biol.* **66** 311 (2013)
146. Powathil G G et al. *PLOS Comput. Biol.* **9** e1003120 (2013)
147. Jalalimanesh A et al. *J. Exp. Theor. Artificial Intelligence* **29** 1071 (2017)
148. Moreau M R et al. *Int. J. Microbiol.* **29** 8868151 (2021)
149. Kuznetsov M, Kolobov A *Mathematics* **8** 1204 (2020)
150. Liu Y et al. *Theranostics* **8** 1824 (2018)
151. Wälzlein C et al. *Phys. Med. Biol.* **59** 1441 (2014)
152. Gao J et al. *Int. J. Cancer Ther. Oncol.* **2** 359 (2014)
153. Kwon J et al. *Int. J. Med. Phys. Clin. Eng. Radiat. Oncol.* **4** 49 (2015)
154. Lin Y et al. *Phys. Med. Biol.* **59** 7675 (2014)
155. Lin Y et al. *Phys. Med. Biol.* **60** 4149 (2015)

156. Azarkin M, Kirakosyan M, Ryabov V *Int. J. Mol. Sci.* **24** 13400 (2023)
157. Ahmad R et al. *Phys. Med. Biol.* **61** 4537 (2016)
158. Cho J et al. *Phys. Med. Biol.* **61** 6 2562 (2016)
159. Verkhovtsev A V et al. *J. Phys. Chem.* **119** 11000 (2015)
160. Tran H N et al. *Nucl. Instrum. Meth. Phys. Res. B* **373** 126 (2016)
161. McMahon S J *Phys. Med. Biol.* **64** 01TR01 (2019)
162. Withers H R *Adv. Radiat. Biol.* **5** 241 (1975)
163. Hufnagl A et al. *DNA Repair* **27** 28 (2015)
164. Alexander P *Trans. New York Acad. Sci.* **24** 966 (1962)
165. Welter M, Rieger H *PLoS ONE* **8** e70395 (2013) https://doi.org/10.1371/journal.pone.0070395
166. Wu M et al. *J. Theor. Biol.* **355** 194 (2014)
167. Stamatelos S K et al. *Microvascular Res.* **91** 8 (2014)
168. Herring N, Paterson D J *Levick's Introduction to Cardiovascular Physiology* (Boca Raton, FL: CRC Press, 2018)
169. Jain R K, Tong R T, Munn L L *Cancer Res.* **67** 2729 (2007)
170. Kuznetsov M B, Kolobov A V *Int. J. Mol. Sci.* **24** 11806 (2023)
171. Cabral H et al. *Nat. Nanotechnol.* **6** 815 (2011)
172. Kuznetsov M, Kolobov A *Russ. J. Numer. Anal. Math. Model.* **38** (5) 303 (2023)